UNIVERSITY OF CALIFORNIA SAN DIEGO

Mangroves from the Sky: Comparing Remote Sensing Methods for Regional Analyses in Baja

California Sur

A Thesis submitted in partial satisfaction of the requirements

for the degree Master of Science

in

Marine Biology

by

Katherine L Qi

Committee in charge:

Professor Octavio Aburto, Chair
Professor Andrew Barton
Professor Ryan Kastner

2021

The thesis of Katherine L Qi is approved, and it is acceptable in quality and form for publication on microfilm and electronically.

University of California San Diego

2021

DEDICATION

This thesis is proudly dedicated to:

My mom and dad, who immigrated to America and gave me the life they always dreamed of. My passions and goals would not be possible without your encouragement and support.

My husband, for being my biggest fan and staying by my side through all the late nights.

Dr. Octavio Aburto, Astrid Hsu, and Dr. Ryan Kastner, for your mentorship, great advice, and allowing me take over the lab computer for the past 3 years.

All the lab undergraduates, for your countless hours of detailed labelling.

My 10th grade chemistry teacher, who didn't believe that marine science was a real career.

TABLE OF CONTENTS

LIST OF FIGURES

LIST OF TABLES

LIST OF GRAPHS

ACKNOWLEDGEMENTS

I would like to thank Dr. Octavio Aburto for his guidance and support through my years as an undergraduate and a graduate student in the Aburto Lab. I would also like to thank Astrid Hsu for all her mentorship and advice with this project and my career aspirations, Ryan Kastner for allowing me to participate in the Engineers for Exploration program and for utilizing many of your computational resources, and Exequiel Ezcurra for your vast knowledge and help in statistics and ecology.

ABSTRACT OF THE THESIS

Mangroves from the Sky: Comparing Remote Sensing Methods for Regional Analyses in Baja

California Sur

By

Katherine L Qi

Master of Science in Marine Biology

University of California San Diego, 2021

Professor Octavio Aburto, Chair

Consequences of global warming are causing mangrove migration from tropical habitats towards temperate zones. Forests at limits and transition zones are important to monitor for promoting local management and conservation efforts. The advancement of remote sensing technology in the past decade has allowed more insight into these habitats at large scales, and recent studies using satellite imagery have succeeded in creating baselines for global mangrove extent. However, the high surveying range comes with a cost of reduced resolution, causing gaps

in areas with high fragmentation or low canopy height, such as in dwarf mangrove habitats. By using drones, we were able to conduct detailed analyses of canopy height distribution for dwarf mangroves in Baja California Sur. This new model provides a focused approach at analyzing parameters that contribute to the multidimensionality of mangrove forests with primarily remote sensing data. Additionally, improved biomass models were constructed with the drone data and compared against satellite data. Due to its inaccuracies in approximated mangrove extent and canopy height, satellite imagery significantly underestimates above ground biomass and carbon measurements in this region, and potentially dwarf mangroves in general. The pairing of satellite and drone imagery allows for a more robust view of mangrove ecosystems, which is critical in understanding their poleward movement with respect to climate change.

INTRODUCTION OF THE THESIS

`   Mangroves are coastal tree species that can thrive in shallow ocean water, populating

subtropical and tropical shores from Mexico to Indonesia. Occupying a small proportion of

Earth's surface area, these forests supply an important contribution that lies beyond what be can

physically seen: their productivity and accumulation of carbon storage (Churma et al. 2003;

Dontao et al. 2011). Known as a major blue carbon sink, wetland ecosystems hold strong

potential for mitigating climate change by long term sequestration of carbon and are more

efficient than most terrestrial forests by area (Mcleod et al. 2011; Hiraishi et al. 2014; Howard et

al. 2017). Furthermore, mangroves provide crucial ecological services to local communities,

including but not limited to protection from erosion and tropical storms habitats for fisheries,

hotspots for biodiversity, and zones of sociocultural importance (Alongi 2002; Moberg and

Rönnbäck 2003; Walters et al. 2009; Polidoro et al. 2010). Nonetheless, mangrove loss has been

prolific due to urbanization, pollution, aquaculture, and lack of political enforcement (Valiela et

al. 2001, Alongi 2002). Over the last 50 years, an estimated third of the global mangrove extent

has been decimated, resulting in about millions tons of carbon released back into the atmosphere

(Alongi 2002). This event is compounded with the combination of other future anthropogenic

inputs and long term consequences of removing a prominent carbon sink.

        To study mangrove forests, scientists have developed a variety of efforts to collect data

on growth, biomass measurements, carbon accumulation, and more. Traditional field work

involve directly going into forests and gathering data by destructive methods. Due to high tree

density and tidal inundation in these habitats, collecting a robust number of samples are labor

intensive and time consuming. Development of remote sensing techniques have enabled

alternatives to ground work, one of which includes satellite imagery. Satellites can map large

swaths of regions and frequently monitor them from a distance, and baseline estimates of total extent, canopy height distributions, biomass, and carbon measurements can be established with allometric equations (Simard et al. 2019). But, the wide coverage comes with a disadvantage of reduced resolution, which can yield significant error ranges (Giri 2016; Lagomasino et al. 2016) These can impact contributors in calculating biomass and carbon results, such as measured mangrove extent and canopy height estimations.

On the other hand, the recent advancement and production of commercial drones has made them relatively low cost and easy to obtain. Furthermore, their ease of use and ability to yield high quality images makes them an efficient tool for surveying sites on a regional scale (Ruwaimana et al. 2018). Conversely to the caveats with satellites, the high resolution costs time and data storage as flying over large areas can be unfeasible. However, the pairing of both instruments to analyze different resolutions of imagery provides a powerful approach at understanding mangroves at both global and regional levels. These insights can not only help researchers understand how ecosystems are currently changing, but also provide data needed to model future changes. Predicting and anticipating shifts within these ecosystem distributions and associated services can inform climate adaptation and mitigation policies for local communities.

Most mangrove species grow between latitudes 30ºN and 30ºS, with the tallest trees occupying equatorial regions (Simard et al. 2019). Generally, mangrove height tends to decrease closer to more temperate zones, and these general patterns have been recorded by large scale global analyses by satellite data (Simard et al. 2019). On a local scale, environmental and geophysical drivers have a large role in spatial variability. Important hydrological parameters, such as proxies to salinity and waterline complexity, can also be distinguished and interpreted for detailed analyses on mangrove distributions (Twilley et al. 1999). In dwarf mangrove habitats,

the forest structure can be more fragmented and with shorter trees than their tropical counterparts. By incorporating these environmental factors in modelling mangrove growth and distribution, we can better understand their ecological drivers as dwarf mangroves still serve as a major carbon sink in their respective regions (Ezcurra et al. 2015). Thus, the study of mangroves at latitudinal extremes validate their importance for conservation and understanding implications of climate change.

As global warming trends continue, temperate ecosystems have seen a gradual shift in dominance to tropical species (Vergés et al. 2014). This phenomenon is known as tropicalization, and mangroves have also been documented to establish themselves in historically temperate ecosystems (Saintilan et al. 2013; Cavanaugh et al. 2014). More specifically, the rise in sea level and decrease in cold weather events in regions that previously lacked mangroves can be partially attributed to their migration (Fazlioglu et al. 2020). Detailing the movement of mangrove forests is crucial for local management as regional responses to their distribution varies widely. As such, monitoring mangroves at the limits of their distribution enables understanding how they will respond to climate change, and how their new establishments will affect adjacent communities.

Chapter 1: Modelling Dwarf Mangrove Canopy Height Distribution

METHODS

Study Site

Data was collected in two locations in Baja California Sur, Mexico: Puerto San Carlos and Ensenada de la Paz. Puerto San Carlos (24° 47' 21.28 " N, 112° 6' 16.32" W) is a small fishing community in Magdalena Bay and faces in the Pacific Ocean. It consists of a coastal lagoon system surrounded by barrier islands offshore and mudflats and deserts moving inland. The climate is desert conditions with rainfall ranging from 48.5 to 153.0 mm per year, depending on seasonal oscillations (Funes-Rodríguez et al. 2007; Rodriguez-Auniga et al. 2013). As of 2010, an estimated 22,312 ha of mangroves populate this region as 3 species: *Rhizophora mangle*, *Avicennia germinans*, and *Laguncularia racemosa*. These species were also present in the second sampling area, Ensenada de La Paz. The lagoons in this region face the Gulf of California, on the southeastern coast of the Baja California Peninsula. La Paz is characterized by arid, desert conditions with an average annual rainfall of about 181.8mm (CONAGUA 2011). In both sites, small, halophilic plants dominate the fringes of mangroves where the soil is drier and more saline. These halophytes tend to grow more inland but can even disperse themselves between mangrove patches where the rarely reaches.

Data collection

Fieldwork was conducted in 2 separate trips in May and July 2018. Quadrat based measurements ($2x2m^2$) were predetermined by random samples within the study site and along transect lines that covered the high-, mid-, and low-intertidal zones. The maximum canopy height (m) was estimated by stacking 1m long PVC pipes to the top of the tallest tree in the

quadrat. A handheld Garmin GPS recorded coordinates at the center of each sample. The basal

diameter (D_{30}) was measured at 30cm for each main root found within the quadrat, along with

the species of the tree. These measurements were later used for validation of data collected by

drone.

Simultaneously to when ground fieldwork was collected, we captured drone imagery

using the 20-megapixel camera on a DJI Phantom 4 Pro. At each site, drone flights were

conducted at 2 altitudes: 120m of entire sites for model reconstruction and 10m of smaller areas

for vegetation verification. The drone took images at 85% overlap in a lawnmower pattern

automatically planned by DJI Ground Station Pro. Calibration images were taken prior to and

after each flight with a gray calibration card to ensure the color scale would remain consistent in

case of changing weather conditions. Further recommendations and details of flight management

are described in Hsu et al. 2019.

<p style="text-align:center"><u>Model processing and calibration</u></p>

Raw images from the drone were saved on an SD card and imported onto a computer for

model construction. The photos were first uploaded to Adobe Lightroom to ensure images from

all flights are consistently color calibrated as changes in weather and time of day can cause color

differences. The image of the gray calibration card is used as a reference for synchronization,

and this process is repeated for every set of images per site. After calibration through Lightroom,

any individual photos that had severe reflections or poor quality were reviewed and removed to

prevent anomalies during model construction.

Structure from Motion (SfM), is a technique to create 3-dimensional models by stitching

together identical features in overlapping images and using geometric information from the

camera's location and motion (Westoby et al. 2012). We used Agisoft PhotoScan (v. 1.4.2 or higher) to perform orthorectification using SfM. The images were uploaded into the program and first aligned by generating a sparse point cloud. Any evident outlier points were reviewed and removed to prevent errors from propagating in following steps. Next, dense point clouds were constructed at Ultra-high quality and further reviewed for any outliers. The red blue green (RGB) orthomosaic was built from the resulting DEM with a 3cm (0.03m) pixel resolution.

The DEM was generated from the dense point cloud, representing a site's topography based on data collected from the drone's altimeter. The measurements were taken relatively as the altitude values have an arbitrary offset and are not representative of the true elevation. Using the RGB orthomosaic, the waterline at which the tide was seen was marked and recorded as the new baseline elevation. There were at least 5-6 ground control points marked per model, with more markers for larger sites (Hsu et al. 2021). We used an algorithm to readjust the camera's positions to minimize the offset for the entire model based on the corrected values. After establishing the ground markers and adjusting the point cloud, the DEM was reconstructed along with a new orthomosaic. These new models are a result of the tide calibration process to ensure canopy height values are accurate and representative of ground measurements.

Figure 1.1: Marking Points for Tide Calibration

An example of the elevation reference markers for 1 site set for calibration. The tide altitude is set to 0.70m here along the waterline throughout the site. The offset here is about 27m based on initial arbitrary values, which is readjusted after running our algorithm

Reference — Cameras

Cameras	Longitude	Latitude	Altitude (m)	Accuracy (m)	Error (m)	Yaw (°)	Pitch
DJI_...	-112.088096	24.803135	250.542328	10.000000	162.944809		
DJI_...	-112.087943	24.803226	250.542328	10.000000	163.046258		
DJI_...	-112.087811	24.803305	250.542328	10.000000	163.075695		
DJI_...	-112.087784	24.803323	250.642328	10.000000	163.178056		
DJI_...	-112.087946	24.803530	250.642328	10.000000	163.109950		
DJI_...	-112.088095	24.803428	250.742328	10.000000	163.151933		
DJI_...	-112.088237	24.803342	250.742328	10.000000	163.157379		
DJI_...	-112.088387	24.803253	250.742328	10.000000	163.146326		
DJI_...	-112.088539	24.803163	250.742328	10.000000	163.182645		
DJI_...	-112.088692	24.803074	250.742328	10.000000	163.268938		
DJI_...	-112.088847		250.642328	10.000000	163.207137		

Markers

Markers	Longitude	Latitude	Altitude (m)	Accuracy (m)	Error (m)	Pr
Elevation Reference 1	-112.091132	24.804473	0.700000	0.005000	28.053665	34
Elevation Reference 2	-112.090440	24.803106	0.700000	0.005000	26.830069	34
Elevation Reference 3	-112.089833	24.803793	0.700000	0.005000	26.640946	37
Elevation Reference 4	-112.089204	24.802859	0.700000	0.005000	26.397997	24
Elevation Reference 5	-112.088952	24.802832	0.700000	0.005000	26.827531	17
Elevation Reference 6	-112.090922	24.804291	0.700000	0.005000	27.827832	37
Elevation Reference 7	-112.090049	24.803442	0.700000	0.005000	26.639883	43
Elevation Reference 8	-112.088607	24.802728	0.700000	0.005000	27.226645	13
Elevation Reference 9	-112.091275	24.804655	0.700000	0.005000	28.493574	27

Total Error
Control points

Scale Bars ▼ Distance (m) Accuracy (m) Error (m)

Total Error
Control s...
Check sc...

Model | Ortho

Elevation Reference 9
Elevation Reference 1
Elevation Reference 6
Elevation Reference 3
Elevation Reference 7
Elevation Reference 2
Elevation Reference 5
Elevation Reference 8

-19.9 m
-26.4 m
-32.9 m

57 m

N
E

Console

```
2021-02-17 13:26:11  Camera DJI_0090 - Old Z: (223.4269785152987) New Z: (250.6423277202184)
2021-02-17 13:26:11  Camera DJI_0091 - Old Z: (223.4269785152987) New Z: (250.6423277202184)
2021-02-17 13:26:11  Camera DJI_0092 - Old Z: (223.5269785152987) New Z: (250.7423277202184)
2021-02-17 13:26:11  Camera DJI_0093 - Old Z: (223.5269785152987) New Z: (250.7423277202184)
2021-02-17 13:26:11  Camera DJI_0094 - Old Z: (223.5269785152987) New Z: (250.7423277202184)
2021-02-17 13:26:11  Camera DJI_0095 - Old Z: (223.6269785152988) New Z: (250.8423277202184)
2021-02-17 13:26:11  Camera DJI_0096 - Old Z: (223.6269785152988) New Z: (250.8423277202184)
2021-02-17 13:26:11  Camera DJI_0097 - Old Z: (223.6269785152988) New Z: (250.8423277202184)
2021-02-17 13:26:11  Camera DJI_0098 - Old Z: (223.6269785152988) New Z: (250.8423277202184)
2021-02-17 13:26:11  Camera DJI_0099 - Old Z: (223.6269785152988) New Z: (250.8423277202184)
```

Console | Jobs

Workspace | Reference | Photos

<u>Mangrove labelling</u>

Once the RGB orthomosaic is calibrated and reconstructed, it is ready for labelling. We trained human labelers to manually classify mangrove and non-mangrove classes from the aerial models in QGIS version 2.18 or newer. Every annotator underwent extensive training sessions to identify mangroves from drone imagery and distinguish them from other types of vegetation. This involved drawing creating a vector layer, drawing detailed polygons over the orthomosaic raster image, and saving the polygons to their corresponding class. For this study, we used 3 classes: mangrove, water, and soil. These polygons were all reviewed by experts and verified using the 10m imagery as reference. The resulting vector shapefile underwent a final check to correct for any geometric errors that may cause discrepancies in analysis.

<u>Analysis of ecological factors</u>

To study which parameters affect mangrove height, data within the models also had to be collected. The detailed mangrove, water, soil labels were used as part of the simulated sampling for 10 sites. These data were included in the generalized linear model (GLM) used to predict canopy height distribution. All statistical tests and models were calculated using R and RStudio.

One hypothesis affecting height was a tree's minimum distance to water, as this can act as a proxy for salinity (Lugo and Sneakder 1974; Cintron et al. 1978; Schmitz et al. 2009). To distinguish the mangrove class from soil and water, all mangrove polygons were first extracted from the label shapefile. The resulting layer was mangrove only, and this was used as the mangrove extent. 250 points per site were randomly sampled within each site's labelled mangrove extent, and the distance in meters to the nearest water label was recorded. This was done with a Shapely function in Python that uses an expanding circle's radius to find the minimum length from a point to the perimeter of a water polygon. With this function, the

distance to water was found for each sample and aggregated into a dataset with its corresponding

site.

The complexity of a forest's waterline was considered as an influence on height. Coastline fractal dimension is a measurement of how smooth or irregular the extent the coast is, as higher dimensions indicate more complexity and lower dimensions are more regular. This is estimated by using 2 different length rulers to measure the length of a coastline, then using their scale factor to calculate the dimension. These equations are described below:

$$N = \frac{ruler_1}{ruler_2} * \frac{length_{ruler_1}}{length_{ruler_2}}$$

Equation 1.1: Calculation of how different measurements from 2 rulers are

$$r = \frac{ruler_1}{ruler_2}$$

Equation 1.2: Scale factor for 2 rulers

$$D = \frac{\log(N)}{\log(r)}$$

Equation 1.3: Coastline fractal dimension

Using QGIS 3.4, the coastline for each site was measured twice by 100m and 10m rulers. This was done by setting a fixed length for line features in a vector layer and tracing the waterline seen from the site's orthomosaic. The rulers were traced over main coastline and large creeks, and the total lengths were added together. This was done for every site, and these values were set as factors for step wise modeling (Table 1.1, Table 1.2). The most extreme examples are shown below in Figure 1.2. A threshold distinguishing types of sites was set at 1.1 to classify sites. For

sites with a dimension less than the threshold, their type was set to "coastal", and "creek" was set

for the higher dimension sites.

Table 1.1: Coastal sites and fractal dimensions

All sites with a calculated fractal dimension less than 1.10 and categorized as coastal.

Site	Fractal Dimension
Puerto San Carlos Site 12 2018	1.0197
Puerto San Carlos Site 13-14 2018	1.0351
Puerto San Carlos Site 1 2018	1.0353
La Paz Site 1 2018	1.0478

Table 1.2: Creek sites and fractal dimensions

All sites with a calculated fractal dimension greater than 1.10 and categorized as creek.

Site	Fractal Dimension
Puerto San Carlos Site 8 2018	1.1204
Puerto San Carlos Site 11 2018	1.1321
La Paz Site 5 2018	1.1339
La Paz Site 1 2018	1.1550
Puerto San Carlos Site 3-4 2018	1.1856
La Paz Site 4 2018	1.239

Figure 1.2: Example of coastal fractal dimension measurements

(A) The most complex, fragmented site marked with 10m and 100m rulers and recorded as "creek". (B) Most simple, continuous site labelled as "coastal".

13
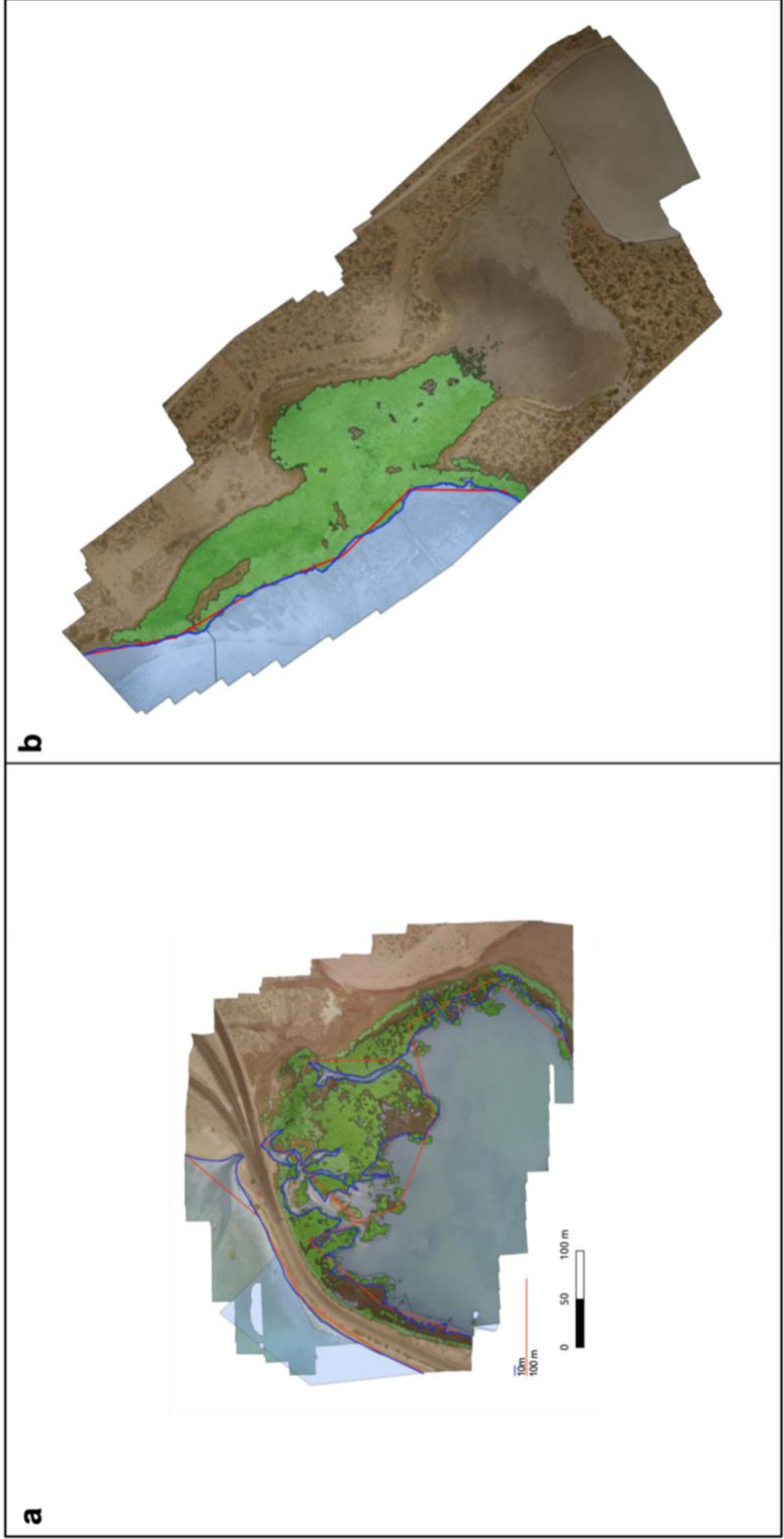
The total coverage of each class was also calculated for each site. Each site's Coordinate

Reference System (CRS) was set to Universal Transverse Mercator (UTM) in the correct zone

(12N). A python script using the Geopandas function for calculating area (m^2) determined the

amount of mangrove, water, and soil was present in each site. The ratios of class to class

(water:mangrove, water:soil, mangrove:soil) was also calculated and included for analysis.

RESULTS

Drone estimated canopy height is significantly correlated to ground measured canopy height

In order to assess whether drone estimates of canopy height can be used, the ground and

drone measurements were compared. The maximum canopy height values from quadrat

sampling were replotted onto the DEM using the GPS coordinates. A simulated quadrat was

drawn for each quadrat sample using QGIS, and the DEM's maximum value was compared

against the field value after removing any outliers with significant GPS or calibration error. A

linear regression indicated a good relationship between drone and ground results, with an R^2

coefficient of 0.74 and an RMSE of 0.54m (Graph 1.1). Furthermore, there is a significant

relationship between the two variables (p-value $\ll 0.01$), and the results of a t-test show no

significant difference in their means (p-value = 0.76).

Graph 1.1: Linear regression results

A comparison between ground and drone measurements, yielding an $R^2 = 0.74$ and an RMSE of 0.54. The blue line is the line of fit while the red line is a reference line. There is a significant relationship between the ground and drone values (p-value $\ll 0.01$).

$r^2 = 0.739$

(x-axis: Ground (m), y-axis: Drone (m))
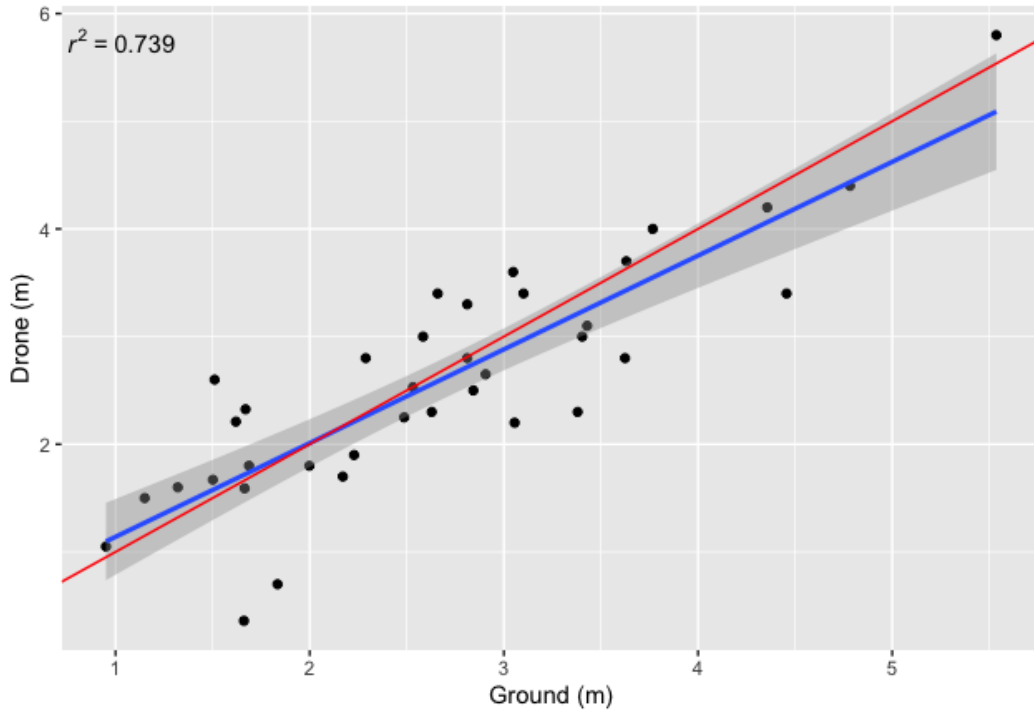
<u>The majority of mangroves are short, near a main body of water, and creek-like</u>

The results of random sampling showed that at over half the sampled mangrove extent was less than 3.5m tall, with a minimum height of 0.02m and a maximum of 9.45m. The mean height found was 3.52m with a standard deviation of 1.68m. At least half of the sampled points were found within 30m of a labelled body of water. The closest points to the water were right along the waterline while some mangroves grew over 220m away from a main water source. The mean distance from water was 42.07m away with a standard deviation of 38.92m. The sites included in this analysis were from Puerto San Carlos and Ensenada de la Paz. From the fractal

15

dimension calculations, 4 sites were labelled as "coastal" and 6 were "creek". These were split

by the established threshold of 1.1 and categorized as factors for model analysis.

The combination of different hydrological and site-specific parameters are significant factors for modelling and predicting mangrove height distribution

Stepwise modeling was conducted to determine the best model given the following

parameters: site location (Puerto San Carlos or La Paz), minimum distance to water, fractal

dimension, site type (coastal or creek), and area of labelled classes (mangrove, water, or soil). A

GLM was run with each variable, one by one, to see which parameters had the most significant

effect. For the canopy height and minimum distance variables, a square root transform was

applied to reduce right skewedness. Comparing against minimum distance aggregated from all

sites, the data is highly variable and show very minor, negative trends by site type (Graph 1.2).

We used a GLM with a gamma distribution as the continuous data was positive and right

skewed. This was determined by checking the model output's residual deviance from the null

and the Akaike information criterion (AIC). After running every combination, the order of

variables for the best GLM was: site location, distance to water, fractal dimension, site type, and

their interactions. Area, along with any of the ratios of coverage, either negatively impacted or

negatively impacted the model. The data split by site level for modelling is shown in Figure 1.3.

Graph 1.2: Prepared data for GLM

The data plotted with square root transformed distance to water (m) and canopy height (m) values. The colors represent the site type categorized by fractal dimension, and the shapes represent the location at which the sample was taken. Lines of best fit were drawn for each site type with slight decreasing trends for both coastal and creek.
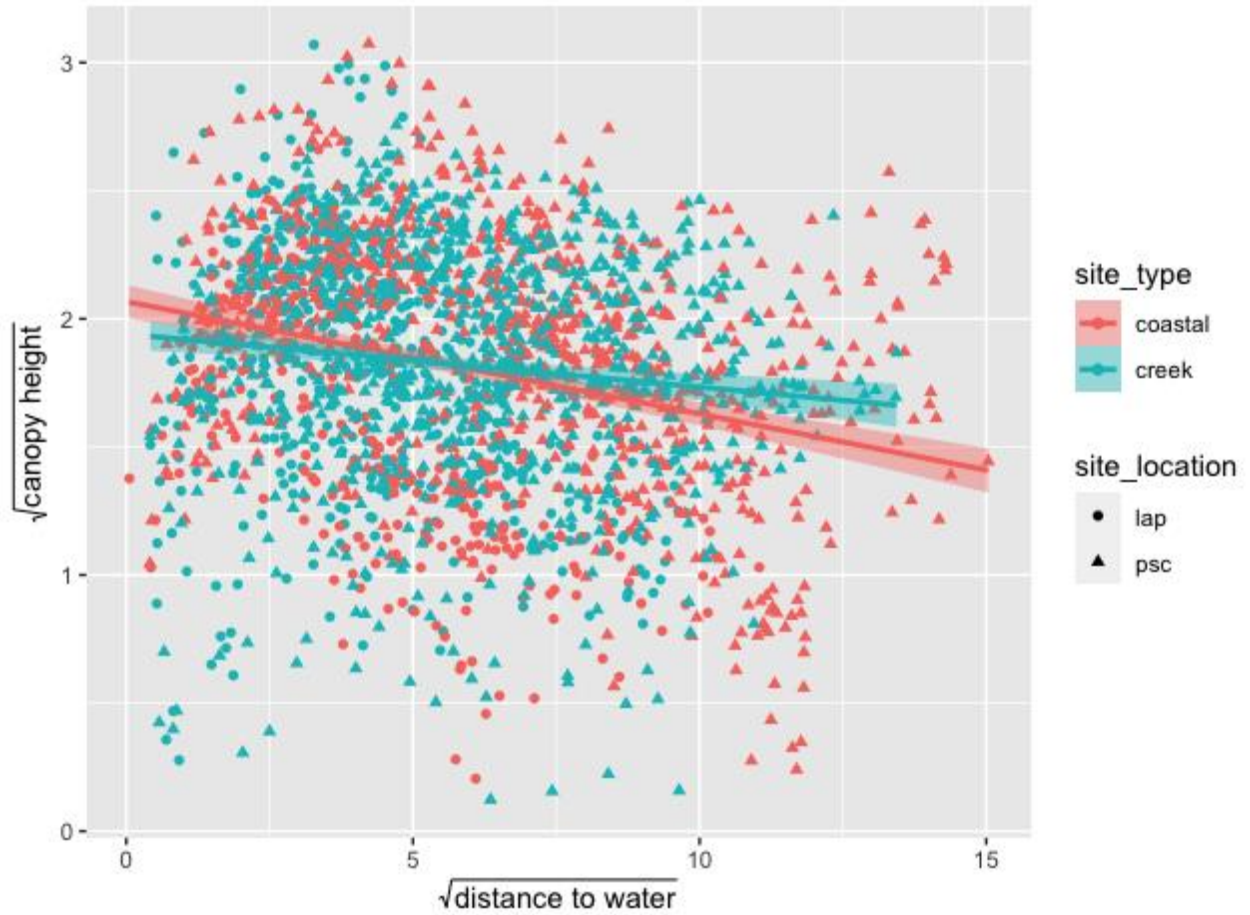
Figure 1.3: Site level variations in order of fragmentation

Each site's relationship with square root transformed distance to water (m) and canopy height (m), arranged in order of least to most fragmented. A line of best fit is drawn through the data with the slope recorded above. A scaled map is displayed alongside by each corresponding graph. The colors indicate the type of site, red for coastal and blue for creek.

Most Continuous

Most Fragmented

site_type
coastal
creek

dimension: 1.1204
slope = -0.038

dimension: 1.0478
slope = -0.15

dimension: 1.0353
slope = -0.043

dimension: 1.0351
slope = -0.041

dimension: 1.0197
slope = -0.1

dimension: 1.239
slope = -0.098

dimension: 1.1856
slope = 5e-04

dimension: 1.155
slope = -0.04

dimension: 1.1339
slope = -0.04

dimension: 1.1321
slope = -0.00041

√canopy height

√distance to water

0m 100m
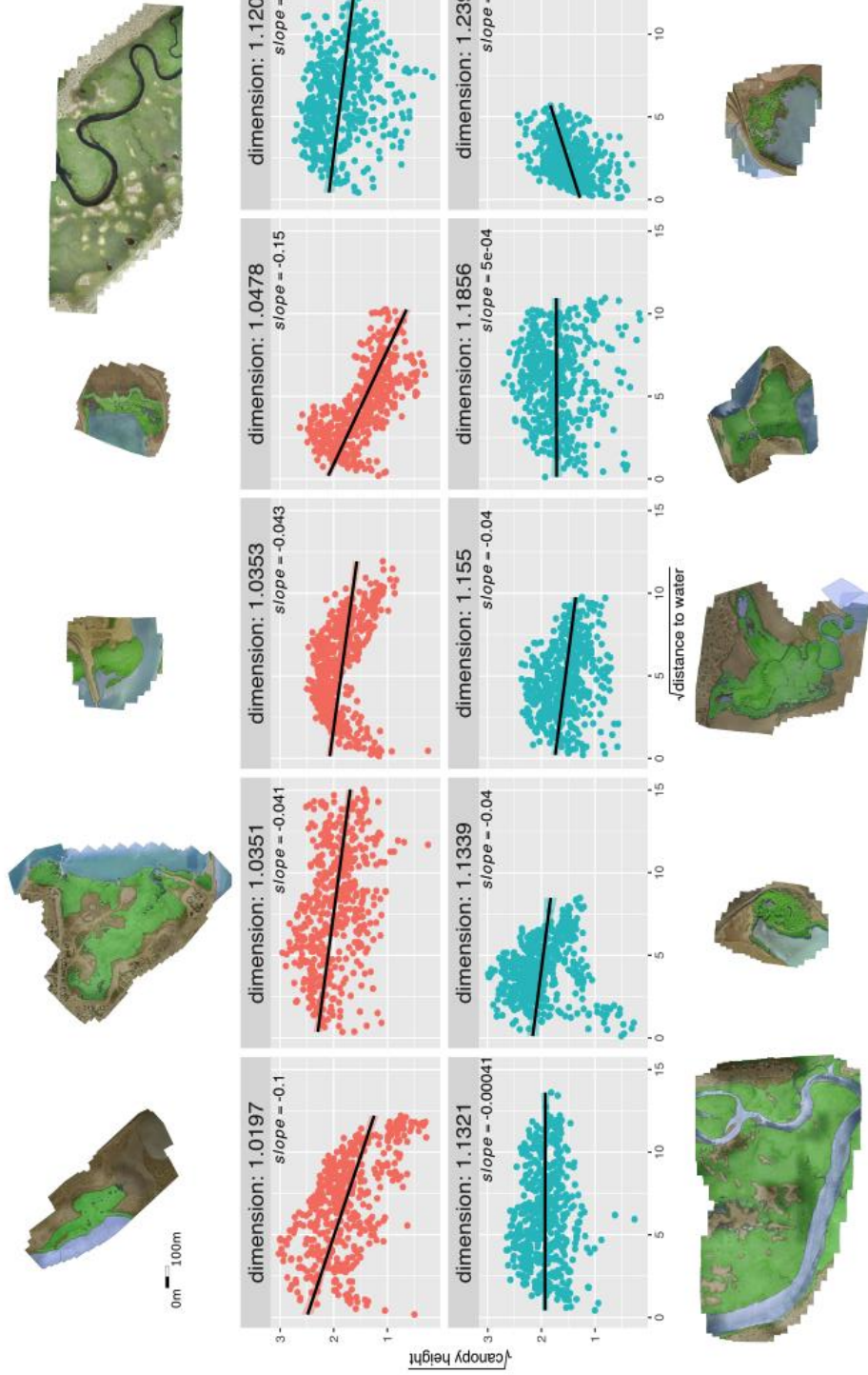
This model had a null deviance of 208.96 and a residual deviance of 159.43. The AIC was

2966.7, which was the lowest score in comparison to all the previous models. A multiple

regressions yielded an adjusted-R^2 of 0.28, which is also the fit of the predicted and observed

results (Graph 1.3). The linear regression for the model's outputs has an RMSE of 0.23.

Graph 1.3: Linear regression model outputs

The observed values plotted against predicted values. The blue line is a line of best fit that goes
through the data. The R^2 is 0.28 with an RMSE of 0.23.
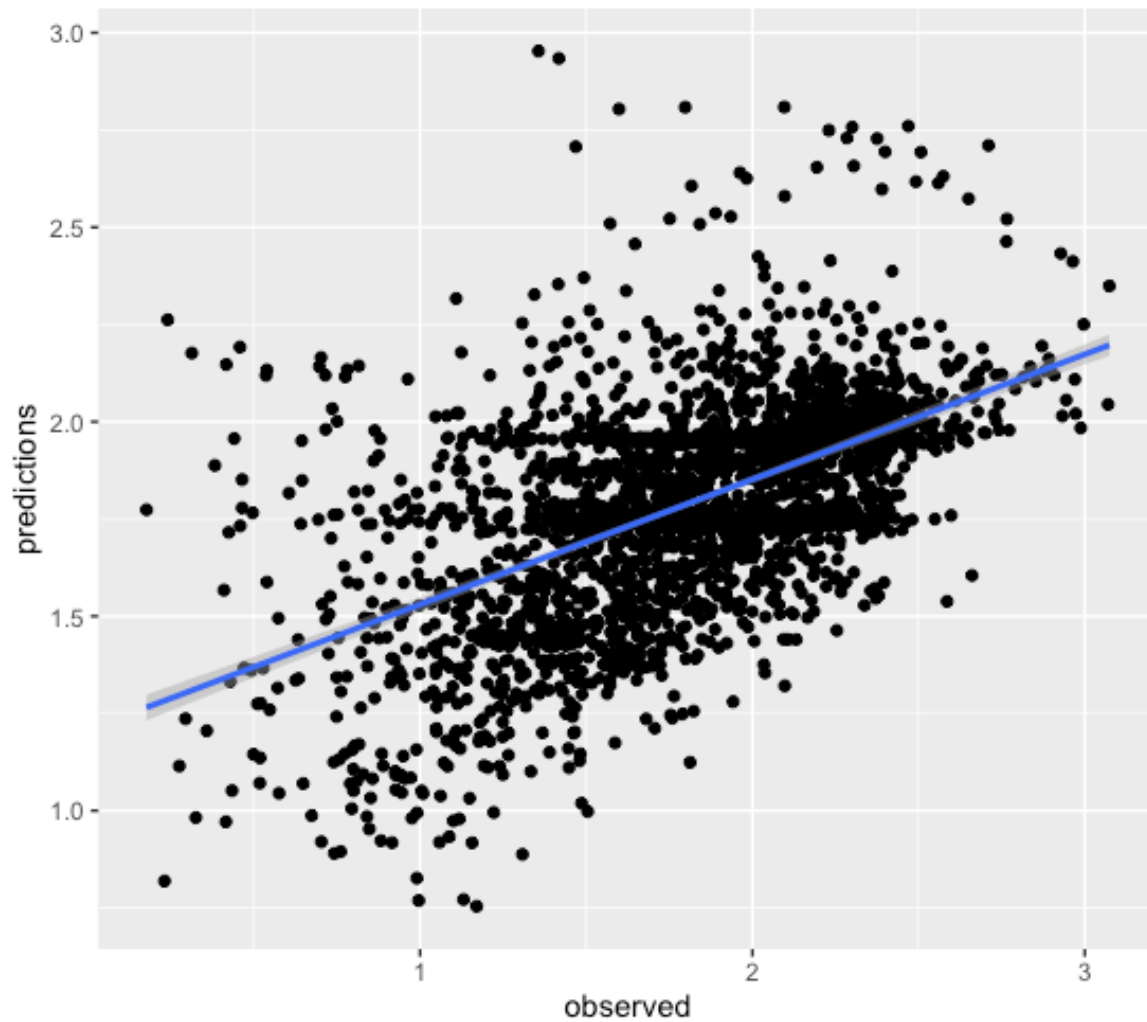
<u>Fractal dimension has a slight positive relationship with the rate of change for distance to water</u>

<u>and canopy height</u>

The slope of the minimum distance to water against canopy height was calculated for each site and compared against the fractal dimension for each site. When split up and arranged by a site level, the derived slope appears to change in steepness with increasing fractal dimension (Figure 1.3). After comparing the slopes with their corresponding dimensions, there is a slight positive trend between the variables (Graph 1.4). There is a low coefficient of determination (R^2 = 0.005) and an RMSE of 0.47. However, fractal dimension has a significant effect on slope (p-value = 0.0006). Thus, these results show a relationship between the complexity of a forest and how canopy height relatively changes with response to distance to water.

Graph 1.4: Relationship of fractal dimension to water distance and canopy height slope

A linear regression each site's fractal dimension against the rate of change for water distance and canopy height. The $R^2 = 0.005$, and the RMSE is 0.47. There is a significant relationship between the two variables with a p-value $= 0.0006$.
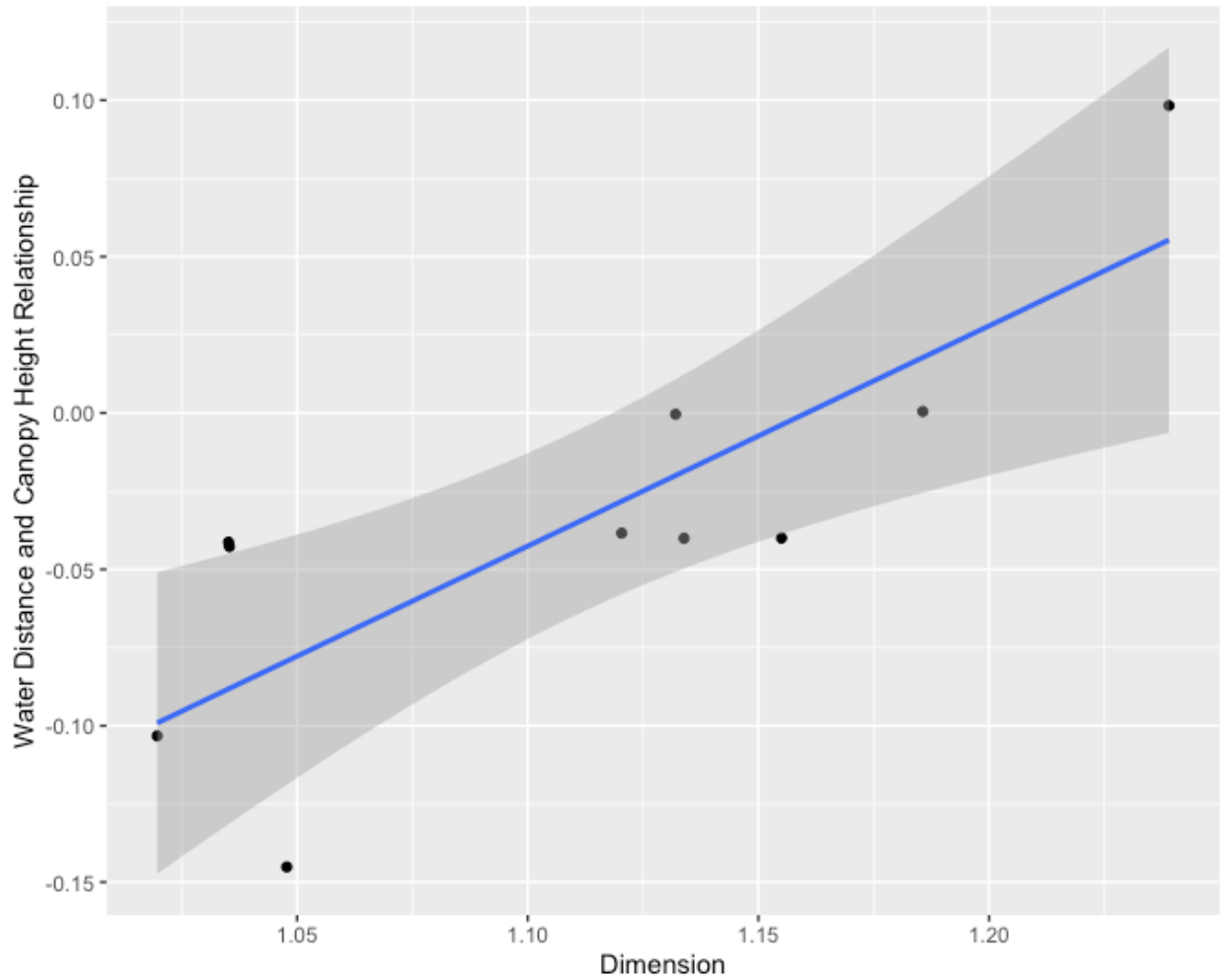
DISCUSSION

<u>Drones are effective for capturing details at high resolution for regional analyses that are</u>

<u>unobservable by satellites</u>

Given the high resolution of the drone imagery, multidimensionality was able to be captured with this level of detail. Several studies have suggested that drones are advantageous over satellite imagery in this regard due to the increase in quality and accuracy of estimations (Ruwaimana et al. 2018, Jones et al. 2019). For this study, using satellite imagery would have been highly ineffective. Label classifications, canopy height estimations, and simulated sampling for collecting ecological data within models would all be affected by larger pixel sizes.

Classifications have improved by coupling satellite labels with drone labels as the increased information can serve as correction factors (Hsu et al. 2020). The higher precision is necessary for conducting site level analyses as variations in smaller, more fragmented forests can hidden from the pixelated view that come with space-borne imagery. Canopy height estimations by satellite would also cause implications in a spatial analysis. Decreased resolution results in larger pixels sizes, which would mask heterogeneity in canopy height fluctuations. This could potentially skew the data to inaccurately represent true canopy height distribution. Further consequences of using reduced resolution imagery for site analyses and dwarf forests are discussed in Chapter 2. Finally, measuring distance to water, coastal fractal dimension, and area per class were possible as the necessary details were visible from drone imagery. For example, the coastline fractal dimension experiment suggested larger ruler sizes influence the measured length of a forest's waterline, especially for complex systems. This is a calculation based on resolution of the measuring tool, and satellite imagery would likely blur features to an extent that

could reduce the difference between lengths by rulers. The continuing pattern of reliance on high

resolution demonstrate the significance of drone usage for regional studies.

Forest complexity signifies underlying hydrological patterns that increase model confusion

A mangrove forest's distribution along the coast is an indicator to how complex it is,

whether it runs along the waterline continuously or is frequently fragmented by creeks and

streams. Salinity fluctuates naturally with seasonal rainfall and tidal patterns, and evaporation in

higher intertidal zones typically result in higher salinity where there is less exposure (Ridd and

Stieglitz 2002; Jolly et al. 2008). Furthermore, increasing salinity has been observed to have an

inverse relationship with mangrove canopy height since more energy must be spent to maintain

internal balance instead of growth (Lugo and Snedaker 1974; Cintron et al. 1978). Using drone

imagery, calculating minimum distance to water was a proxy for salinity measurements. We

expected to see clear patterns with mangrove canopy height and their locations respective to

water but found high variations on a site to site scale (Figure 1.3). Taking coastal fractal

dimension into account, we found that complex systems are harder to predict. When a forest's

waterline is relatively straight and regular, it had a lower dimension and a generally more

negative relationship with water distance and canopy height. The slope represents how canopy

height responds to distance to water, so a negative relationship suggests that taller mangroves are

closer a body of water and shorter mangroves are farther away. This aligns with the findings by

Cintron et al. for their research on salinity effects on mangrove height. However, this pattern is

reduced as fractal dimension increases (Graph 1.4). As water ways become more intricate and

variable throughout a forest, the relationship between distance and mangrove height becomes

less clear. This could be related to water undetected by drone imagery, such as underlying creeks

or ground water flows, that may affect salinity. Potential hidden bodies of water could make the height distribution more homogenous throughout as salinity levels would be relatively stable. Another possibility is anthropogenic impact. Habit destruction is another cause for fragmentation in mangroves as aquaculture, urbanization, and pollution have detrimental effects on forest health (Li et al. 2013; Bryan-Brown et al. 2020). One group found effects on leaf area index and gross primary productivity with respect to different levels of fragmentation (Kanniah et al. 2021). Although fragmentation has been researched with relation to effects on biodiversity and environmental impacts, there are few studies conducted on the consequences of mangrove stocks, especially dwarf mangroves (Tran and Fischer 2017; Corte et al. 2021). Several sites from our study are located near urban structures, such as roads and fishing sites. Instead of naturally occurring fractality, the mangroves may have been fragmented by human influences. The results of our canopy height distribution analysis suggest that fragmented forests are more difficult to predict than continuous sites. These causes are yet to be investigated, but can potentially reveal important contributors controlling for mangrove height.

Inclusion of other parameters detectable from drone imagery may increase model accuracy

The relationship between salinity and canopy height has a strong, negative correlation (Cintron et al. 1978). However, species distribution is also impacted by salinity zonation (). Puerto San Carlos and La Paz have 3 observed mangrove species present. Typically, the general trend follow that *R. mangle* is found in the lower intertidal and more inundated zones, *A. germanins* grows farther inland and can thrive in higher salinity with their pneumatophores, and *L. racemosa* is either usually found in between other species or towards the upper edge of tides

(Kruczynski and Fletcher 2012). These species can have distinct zonation patterns, but they are commonly found to be mixed together as their elevation ranges overlap (Pulver 1976). As salinity affects height distribution, species can also be impacted as different salinity preferences and tolerances cause shifts in dominance. In our models, labelling on the species was not feasible given time constraints. Though the drone imagery has significantly higher resolution than satellite imagery, distinguishing species is still difficult given the density of the forests and heterogeneity of species mixing. We found that species were identifiable at 10m, but labelling their complex shapes over large areas proved to be too time consuming (Figure 4). For this reason, mangroves were labelled as a general category in order to gather more data for analysis. Though generating enough data on species by manual labelling is impractical, it is possible to use automated methods such as machine learning to generate labels. As methods in automatic classification advance, species data could become accessible to use in our current model.

Figure 1.4: 10m resolution image of mixed species

1 image from a 10m flight that captured all 3 species: *R. mangle* (**R**)*, L. racemose* (**W**)*, A. germanins* (**B**). Species are distinguishable from this resolution but are difficult to label as they tend to grow over each other. This is also intensive for manual labelling due their irregular shapes.

In our water labels, all visible water was categorized in one class. This included the ocean, rivers flowing through deltas, and small streams. However, these water bodies may have varying levels of salinity depending on their location and size. Creeks and small ponds farther from the ocean, the main source of water input, are more exposed and susceptible to evaporation. Thus, this environment most likely experiences more fluctuations in temperature, salinity, oxygen levels, and other parameters that affect mangrove growth. If vicinity to all types of water does not equally affect canopy height, this could contribute to the variability of the canopy height distribution. Distinguishing different water sources would require more detailed labelling and

further analysis of hydrological patterns in BCS. However, this is possible with the drone

imagery and can even be incorporated with tidal data. Water labels are created by marking where

all water is present in the orthomosaics, though water presence is dependent on the tide level at

the time the drone imagery was collected. By taking tidal height into account with the types of

water bodies, this can provide information on whether a particular water label is regularly

inundated or only at high tide; when these data are aligned with the randomly sampled points,

this may further our understanding on mangrove height distributions.

Predictors in canopy height can be linked to better understanding biomass and carbon storage of entire sites

Mangrove canopy height is correlated to annual litterfall rates, indices of organic

production and litterfall rates (Saenger and Snedaker 1993). Thus, above ground biomass (AGB)

is intrinsically related to height. Several studies found a significant linear relationship between

height and AGB and were able to calculate estimates of biomass with satellite remote sensing

(Saenger and Sneakder 1993; Simard et al. 2006; Fatoyinbo and Simard 2012). The drone DEMs

used for mapping canopy height distributions can also estimate AGB through established

allometric equations. Additionally, the drone models are at a higher resolution than satellite

imagery. This may increase accuracy in biomass estimations for these particular sites, as they are

predominantly dwarf mangroves and fragmented to a certain extent. As stated in the above

sections, larger pixel sizes reduce the amount of spatial variability that can be detected from

remote sensing models. Further elaborated in Chapter 2, a higher resolution perspective of

canopy height can resolve the errors found in biomass estimations from satellite imagery. As

parameters that control for mangrove height distribution are more understood, better baselines

for biomass and carbon stocks can be established for management and conservation efforts.

Surveying by drone is becoming more accessible through recent technological

advancements and commercialization. Utilizing this machine to collect scientific information can

be a reliable tool for monitoring regional changes. We studied hydrological patterns that were

observable by drone imagery and significantly affected canopy height, such as distance to water

and coastal fractality. These factors may also predict how mangroves will respond to these

changes with tropicalization altering the distribution of wetland vegetation. Additionally,

predicting shifts in growth and movement of mangroves can to climate change induced

tropicalization alters the distribution of forest stands. With the poleward movement of

mangroves at temperate zones, this knowledge can inform climate adaptation and mitigation

policies in local communities.

<div align="center">Uncertainty and error in estimations</div>

Our study spanned over several locations and trips in BCS with various teams of people

working on data collection. Consequently, there were likely slight variations in how

measurements were taken which may have introduced error into our results. One possible source

of uncertainty stemmed from how field measurements of canopy height were taken. We

attempted to conduct this study with non-destructive methods, such as uprooting and cutting

down trees. As most trees did not exceed 4m, we connected and stacked 1m PVC pipes together

to visually approximate the maximum height per quadrat. Quadrat measurements were rotated

within field teams, including height estimations. Thus, there may be inconsistencies in measuring

canopy height if pipes were not properly stacked or if estimation by visual inspection was

difficult due to thick vegetation in high density areas of forests. Additionally, each group used a

handheld GPS to mark the coordinates of each quadrat sample. According to the Garmin manual, the error range is typically 5-10m depending on atmospheric conditions. However, fieldwork was conducted within forests that could potentially interfere with the GPS signal due to the thick, tangled nature of mangrove roots. When comparing ground measurements with model estimations, these sources of error can result in more variability instead of having a perfect linear relationship (Graph 1.1). Nonetheless, there was no significant difference found between the ground and drone heights after quadrats were reviewed for significant GPS errors, and the uncertainty is random. Therefore, our models are still representative of the surveyed sites given the potential errors. Furthermore, they cover more area than the ground measurements in a smaller amount of time, serving as an efficient alternative for ground methods.

During model construction, the DEMs rely on ground control markers to establish set elevation references. Without these points, the models are subject to geometric distortion that result in concave or convex shapes. The canopy height analysis experiment depends on the validity of the DEMs, and inaccuracies from building the models can introduce significant error into the results. Unfortunately, we were unable to collect elevation data at a high enough precision and frequency, so tide calibration points were marked throughout the model to resolve geometric flaws. The algorithm used to readjust camera positions minimized altitude offsets for all the points, though it relied on manually marking where the waterline was visible on the model. The calibration was also completed by trained scientists following a written guideline (cite drone manual here), though the point locations may have varied per person. Any inconsistencies in tide calibration would result in estimated topography errors, affecting the canopy height measurements. Also, the edges of DEMs were typically noisier than the rest of the model due to less overlapping images. SfM relies on identical features dispersed within photos

taken at close vicinities to reconstruct 3D models, and discrepancies would tend to appear more at the edges because there are less surrounding images. Thus, mangroves detected at the edge of DEMs were more likely to have distortions than the trees towards the center of models. These resulted in random over- or under-estimations in canopy height. As described above, the model errors did not a significant effect on the final results. There is a strong correlation between ground and drone height values, and our models are robust enough to handle small geometric errors.

Conclusions

This study utilized drone imagery to conduct site level analyses on mangrove canopy height distribution. Drone and ground data are highly correlated, and estimates from the drone's altimeter can create reconstructions of forest topography. Hydrological parameters can also be observed at the high resolution of drone DEMs, and they can be used as variables for predicting canopy height. It was found that BCS's dwarf mangroves are typically found near the water and can have fragmented coastlines. The level of complexity has a slight significant effect on how distance to labelled water can affect forest's height distribution. This may be attributed to underlying patterns not covered by our experiments, such as water that was unobservable by drone imagery, species distribution, and anthropogenic influences. With these caveats, drones still remain an advantageous method to surveying mangroves for regional analyses. They maintain high levels of accuracy in data collection and can capture spatial variations unseen by space-borne imagery. This study provides a novel method of harnessing drone data for analyzing patterns in mangroves at a fine detail, providing information that can allow scientists to anticipate local changes and shifts caused by climate change.

Chapter 1, in part, is currently being prepared for submission for publication of the material. Qi, Katherine; Hsu, Astrid; Aburto, Octavio; Kastner, Ryan. The thesis author was the primary investigator and author of this material.

Chapter 2: Above Ground Biomass and Carbon Estimations by Satellite and Drone

Imagery

METHODS

Drone data collection and processing

Imagery was collected by flying over each site surveyed by ground as described in Chapter 1. The data was calibrated and constructed into DEMs and RGB orthomosaics using Agisoft, then labelled by trained annotators in QGIS as described in Chapter 1. Mangrove and non-mangrove classes were identified and verified by experts to ensure correctness in classifications. The labels were processed by another script to automatically resolve any geometric or polygon errors from manual labelling. The labels were saved as a polygon vector shapefile that contained all the mangrove and non-mangrove classes. After the tide calibrated DEM and labels were reviewed, the files were ready to be inputted for biomass calculations.

Satellite data processing

Global mangrove satellite data were used from a study published by Simard et al. in 2019. Canopy height maps were generated by 30m resolution from the Shuttle Radar Topography Mission (SRTM) and Geoscience Laser Altimeter System (GLAS) data from 2000. These produced global baseline maps for maximum canopy height and basal area weighted height, the second of which was used for calculating biomass. Biomass was calculated using a specific allometric equation for the North, Central, and South American region (Equation 2.1). Mangrove extent was classified with hybrid supervised and unsupervised techniques from a previous study (Giri et al. 2011). The rasters for maximum canopy height and above ground

biomass maps were downloaded for Mexico and uploaded into QGIS. Each drone map extent

was used to clip satellite layers to extract the observed satellite map for that area. There were 10

surveyed sites from our drone DEMs, and 10 corresponding maps for both canopy height and

biomass data were also generated. Above ground carbon storage was estimated by multiplying

0.451 with biomass, as stated in the IPCC guidelines (Hiraishi et al. 2014). The canopy height

and biomass maps for drone and satellite imagery were used for direct comparisons of each

other.

$$AGB \; = \; 1.418 * H_{ba}{}^{1.6038}$$

Equation 2.1: Allometric equation for estimating AGB (Mg/ha) for SRTM data

Equation derived from linear regression of biomass measurements from field sampling in North, Central, and South America. The R^2 is 0.71 with an RMSE of 54.3 Mg/ha.

Calculating biomass and carbon from drone DEMs

A python script was written to automatically produce biomass maps from DEMs and

mangrove/non-mangrove labels. The labels were separated by class, and the mangrove polygons

were extracted and used to clip over the tide calibrated DEM. The resulting raster was a DEM

that only covered mangrove extent, representative of the canopy height within the flown site.

After the mangrove extent of the DEM was generated, a global, linear allometric equation

(Equation 2.2) was applied over the layer (Saenger & Snedaker, 1993). The resulting layer is in

units of Mg per hectare, which can also be used to determine total biomass of the surveyed

sites. This script is available on a public GitHub repository (Qi 2021), and detailed steps to run it

are outlined on the Wiki page.

$$10.8 * Canopy\ Height\ (m)\ +\ 34.994$$

Equation 2.2: Global allometric mangrove biomass (Mg/ha) equation

General equation reported from Saenger and Snedaker 1993. A linear regression of biomass measurements spanning from mangroves in various latitudes reported an R^2 of 0.774 and a significant relationship ($p < 0.001$) between canopy height and AGB.

To calculate total biomass (Mg) of a site, a conversion factor must be multiplied against the biomass layer's cell values (Mg/ha). This is determined from the area of the pixel, the layer's smallest element (expressed in units of m^2), which can be found using the resolution of raster. For example, if the drone's resolution is 3.125, its total area expressed in ha would be 9.766 x 10^{-8}. The product of the summation of all biomass pixels in the biomass layer with this factor is the total biomass expressed in Mg. Carbon estimates were calculated from the resulting AGB maps. Following the IPCC guidelines, carbon storage was estimated to be about 45.1% of the calculated biomass (Hiraishi et al. 2014). This conversion factor was multiplied across the total biomass found for each site to estimate the total amount of carbon stored above ground.

$$1\ ha = \frac{resolution\ (m)}{210000}$$

Equation 2.3: Biomass conversion factor from meters to hectares

Grid sampling over drone and satellite models

To directly assess the drone and satellite results and their differences, each model was sampled using the same technique and extent. A fishnet grid of 30m squares was generated over each model to represent the pixel resolution of the satellite data. For reference, each grid would contain 1 satellite pixel or up to 100,000 drone pixels for 3cm resolution. Each site shared the

same fishnet grid to maintain consistency across instruments. This was done for canopy height and biomass maps for both drone and satellite data using a Python script with the Geopandas and Rasterio libraries. Thus, grids would be taken from 4 models for 10 sites, resulting in samples that spanned across 40 different models. The minimum, maximum, mean, count, and standard deviation of all values were taken within each sample and exported for statistical analysis in R. Each instrument's canopy height and biomass maps shared the same extents, and the corresponding types of maps were compared to each other by instrument. Additionally, the amount of SRTM labelled mangrove extent was cross-referenced with the drone's non-mangrove labels to check how much non-mangrove area was labelled as mangrove. This was done by calculating the amount of area labelled as non-mangrove by drone but labelled as mangrove by SRTM, which will be referenced as 'true non-mangrove'.

The satellite data had varying extent from the drone's due to its lower resolution. Detailed ecological variations could not be distinguished between as satellite pixel size was too large (Figure 2.1). Consequently, non-mangrove classes were sometimes categorized as mangrove within satellite images. These edge cases may have an effect on the direct comparisons of drone to satellite data. To test this concept, the same fishnet grids were applied to both drone and satellite mangrove extents for the biomass models. However, samples were only recorded when a grid was completely filled with drone mangrove pixels. This ensured that direct comparisons would not be biased if sample sizes per instrument differed. The same statistical tests and analyses were also run on these grids using R.
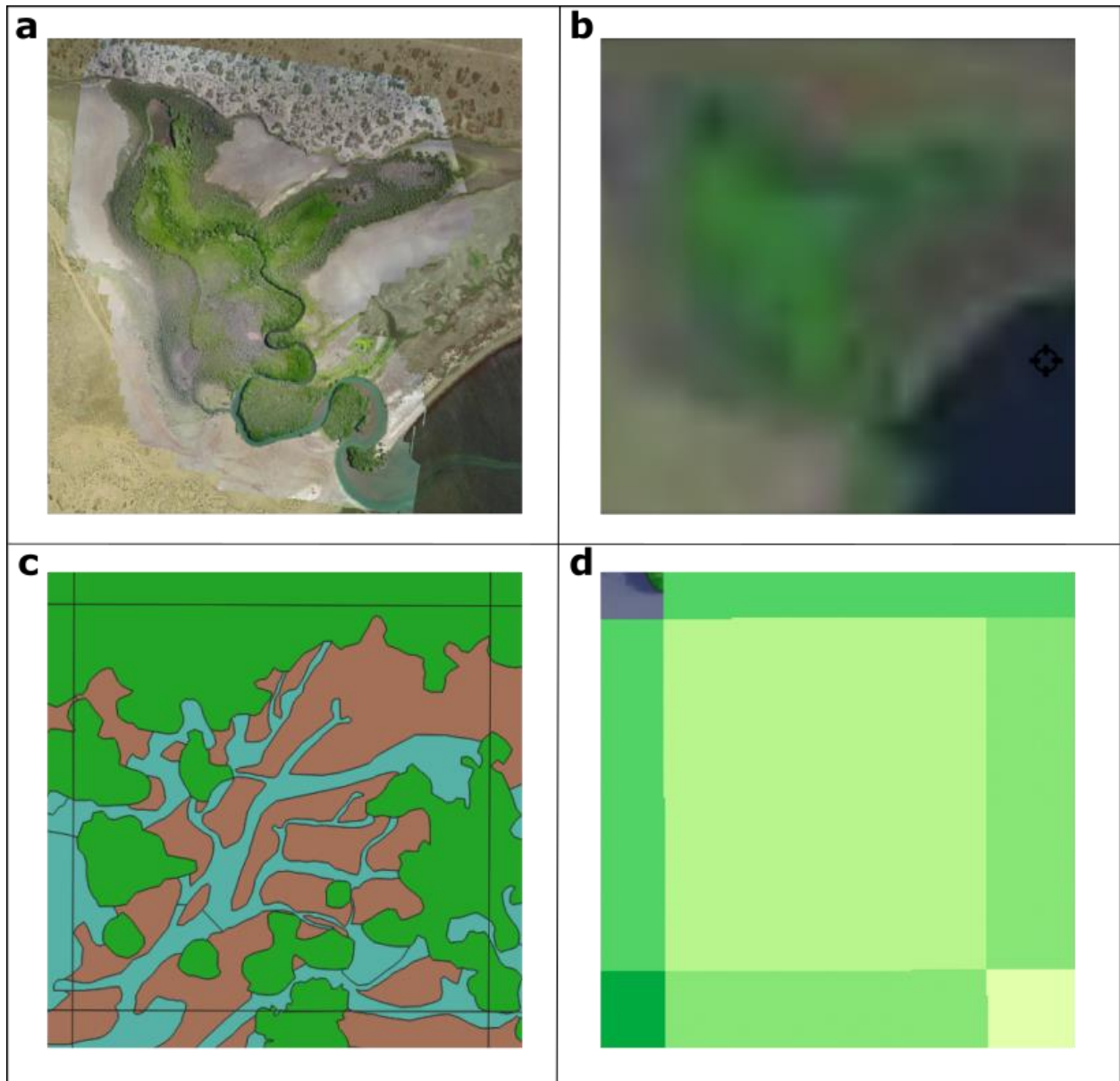
Figure 2.1: Comparison of resolution by instrument

The differences of mangrove detection from drones (a, c) and satellite (b, d). (a) An RGB orthomosaic of a site in La Paz taken by 3cm resolution drone imagery. (b) Landsat satellite view of the same site in panel (a) with 30m resolution. (c) A 30x30m grid showing mangrove (green), soil (brown), and water (blue) labelled with drone imagery. (d) The same grid in panel (c) classified as only mangrove by satellite data.

RESULTS

Measured mangrove extent depends on site size and instrument type

The resolution differences between drone and satellite imagery is about 1000x in magnitude (0.03 m and 30 m). Thus, there are disparities between the amount of area covered by instrument due to over- or under-estimations by SRTM data. To check mangrove labels for SRTM imagery, the proportion of true non-mangrove labelled as mangrove by SRTM was 16.56% for all the sites. The mean ratio of true non-mangrove to SRTM mangrove was 25.48% $\pm$ 18.83%. By individual sites, the amount of area ranged from 0.05% to 62% of a total site. The total measured area (ha) was measured by summing the number of grid samples per instrument and multiplying it against the size of the sample (0.09 ha). Overall, the drone imagery measured 168.31 ha, and SRTM measured 106.76 ha. There was no significant difference between the variance of each area distribution, so a two sample t-test was run for all the samples per instrument. There was not a significant difference in the total amount of area found for drone and SRTM data (p-value = 0.33), though there appeared to be site to site differences (Graph 2.1a). Given that the drone imagery was a much higher resolution, it was used as a baseline to determine the relative size of each site. In panel a of Graph 2.1, the sites are arranged by increasing measured drone area (left to right), and the difference in measured area by instrument seems to widen as drone area increases. The sites were then categorized into different size classes given their respective drone area estimations: "small" for sites $\leq$ 5 ha, "medium" for sites > 5 ha and $\leq$ to 20 ha, and "big" for sites > 20 ha. The differences between drone and SRTM area by site were plotted and grouped together by their corresponding size classes in Graph 2.1b. There is a general increase in differences as site size increases. Big sites can have over 15 ha of difference between drone and SRTM extents, whereas differences in smaller sites are near 0.

Graph 2.1: Measured area by instrument and their site level differences

(a) The total amount of measured area (ha) by site and instrument, arranged in increasing order of drone area. The pink represents drone data while the purple is SRTM. (b) Differences between drone and SRTM measured area by site and grouped by size class. Red represents the small sites ($\leq$ 5 ha), green are the medium sites (> 5 ha and $\leq$ 20 ha), and blue are the big sites (> 20 ha).
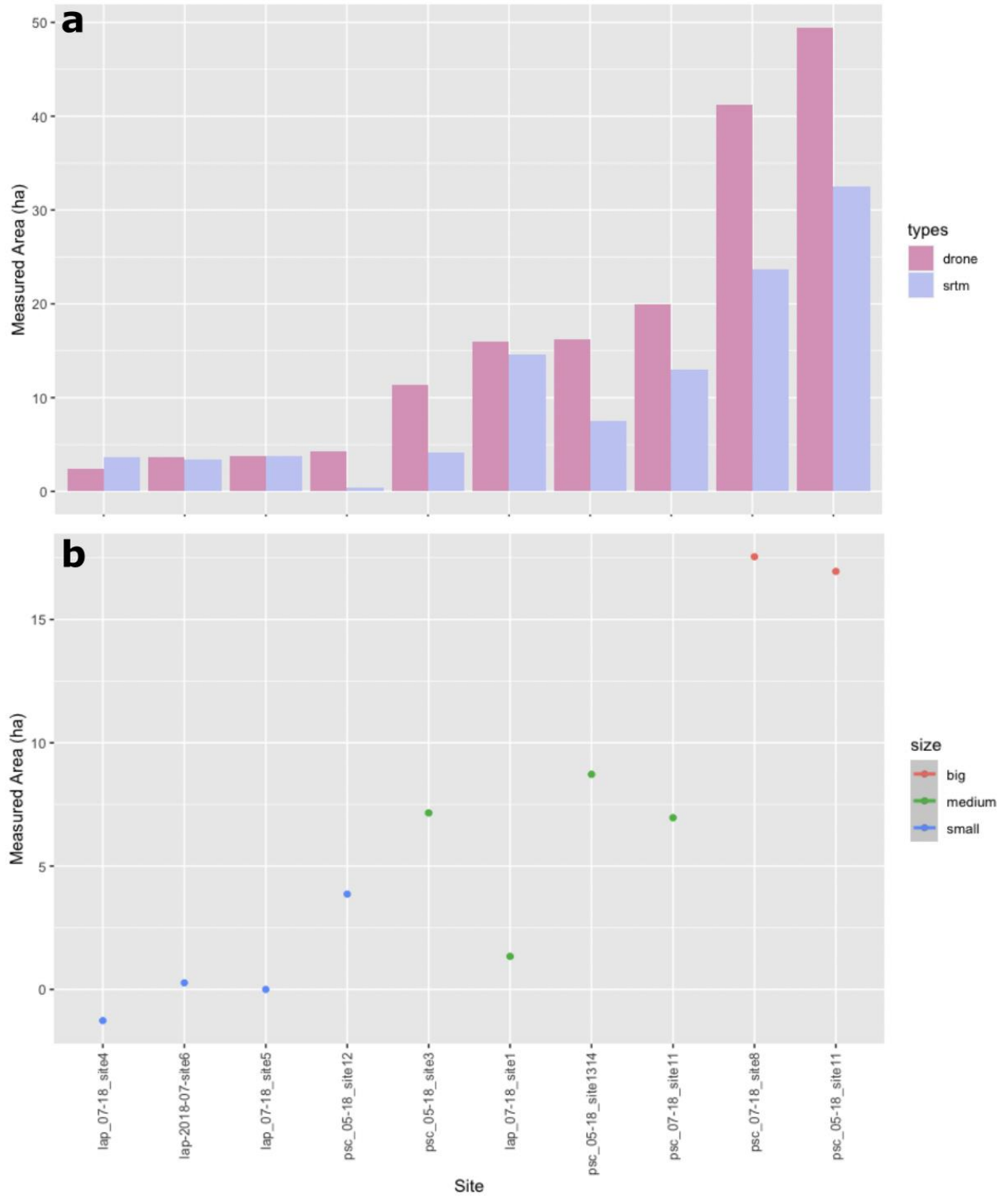
A two-way ANOVA by size class and instrument type was run after establishing normality and equal variance, and there was a significant interaction effect for the factors (p-value = 0.009). A post-hoc test (Tukey-Kramer) was run to determine which groups were different which are indicated by letters (Graph 2.2). Letters that are the same represent groups that are not significantly different from each other. There were no significant differences found between area by instrument for the small size class (p-value = 0.99). In the medium class, there was also no significant difference found between instruments (p-value = 0.25), but the SRTM medium extent was not statistically different from either the drone (p-value = 0.21) or SRTM area (p-value = 0.14) in the small class. There was a significant difference between measured mangrove area in the big class for SRTM and drone (p-value = 0.004). Overall, the drone data had significantly different measured areas by each size class while the SRTM data only had a difference between its big and small/medium classes.

Graph 2.2: Tukey-Kramer test results on extent by size class and instrument

The total measured area by small, medium, and big sites. The types of instrument are distinguished by color, and the letters represent which groups are significantly different from each other. These groups are: small drone, small SRTM, and medium SRTM; medium drone and medium SRTM; big drone; big SRTM.
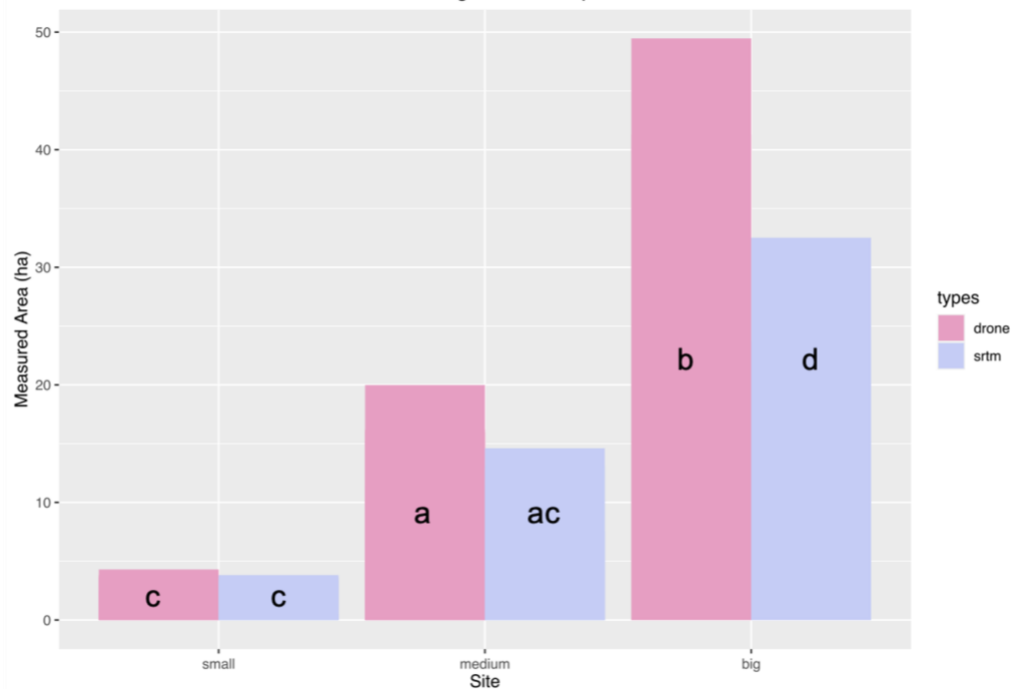
Canopy height measured by satellite and drone are significantly different

After aggregating all the canopy height samples together, there were 3,047 drone samples and 1,232 satellite samples. The satellite maps were constructed using the maximum canopy height derived from SRTM data (SRTMH$_{max}$), and SRTM will be used to refer as satellite results in the remainder of this chapter. As such, the maximum height for each drone sample was compared against each of the SRTM results to maintain consistency. The frequency distribution of maximum canopy height for both instruments showed the satellite data right skewed of the drone data (Graph 2.3). The mean canopy height per sample for drone data was 5.18 m with a

standard deviation (SD) of 2.11. The shortest tree found was 0.43 m where as the tallest was

17.18 m. Over half of the detected mangroves were less than 5.1 m tall. On the other hand,

SRTM samples had a mean of 2.77 m (SD = 2.04 m). The canopy height ranged from 0.54 to

15.06 m , and at least 50% of the detected mangroves were under 2.2 m. A Welch's t-test

confirmed reported that canopy height measured by satellite and drone are significantly different

from each other (p-value << 0.01).

Graph 2.3: Distribution of maximum canopy height by instrument

The frequency of canopy height for all grid samples, categorized by drone (red) or SRTM (blue).
The dashed lines represent the mean of each dataset, 5.18 ± 2.11 m for drones and 2.77 ± 2.04
m for SRTM.
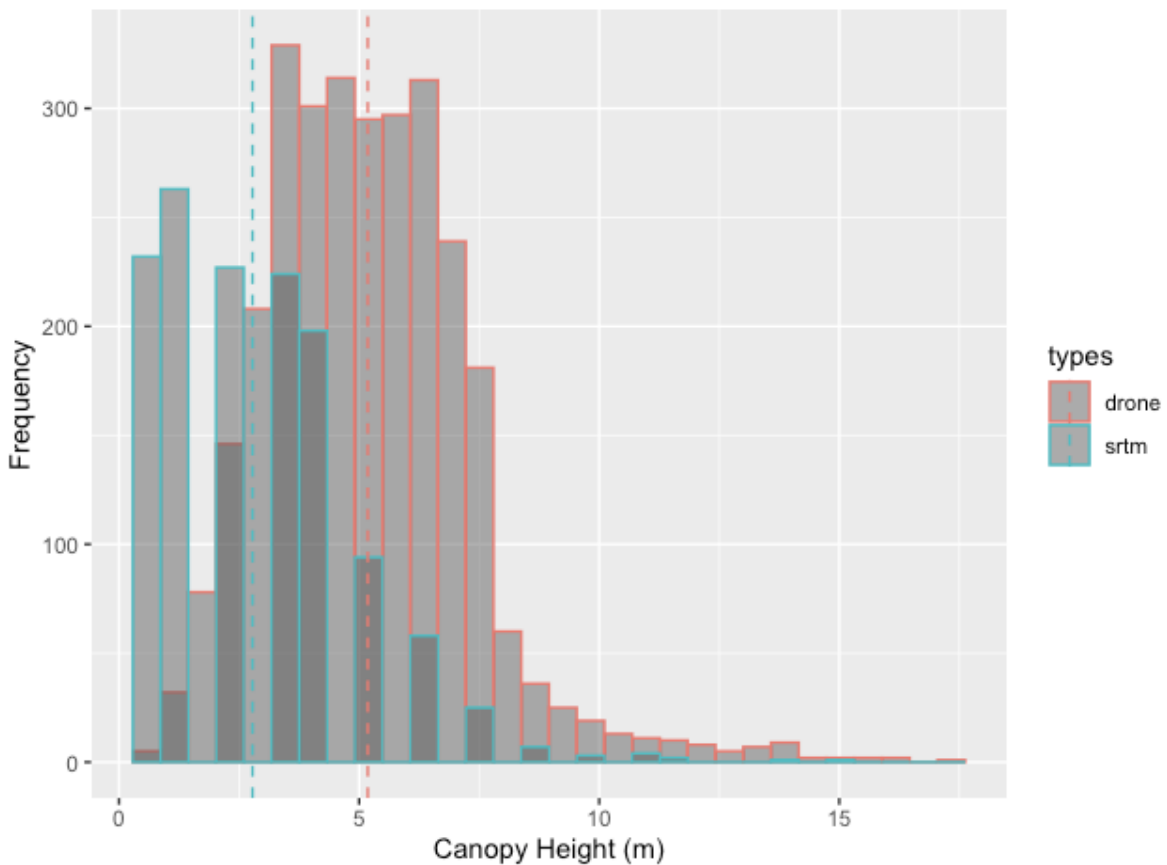
Since the size of each site had a significant effect on measured mangrove extent, canopy height estimations were also tested by this factor to see if it had an effect. The mean of each sites sampled max height was taken and plotted by increasing area (Graph 2.4a). There was not have a visible pattern with height estimations by instrument, and 4 out of 10 sites had a higher estimated mean height for SRTM than drone. The sites were grouped into "small", "medium", and "big" categories again by the same parameters defined in the mangrove extent analysis. The mean height was then taken by size class for both drone and SRTM (Graph 2.4b). For drones, the mean height for "small", "medium", and "big" classes in respective order were: 4.91 m, 5.33 m, and 5.10 m. For SRTM, these were 4.62, 2.94, and 2.02 m. There appeared to be a slight decrease in SRTM canopy height as site size increased, while drone canopy height did not a visible relationship. After checking the assumptions, an ANOVA was run to check for main effects and interactions between size of site and instrument used. There was no significant interaction effect found for interactions (p-value = 0.28) or size (p-value = 0.45). There was a slight significant effect on the type of instrument used (p-value = 0.031).

Graph 2.4: Mean canopy height by site and size class

(a) Mean max canopy height arranged by site in increasing order of area (left to right).
Pink represents drone samples, and purple represents SRTM. (b) Mean max canopy
height arranged by size class (small, medium, and big).
(b)
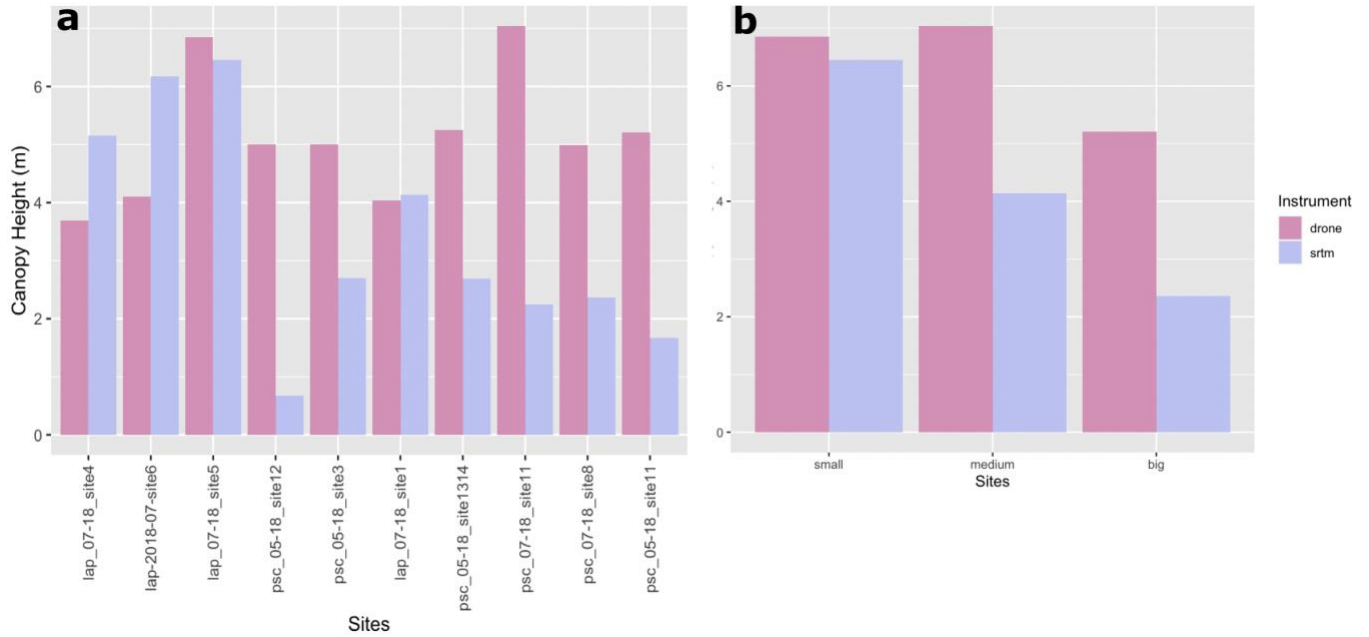
Biomass and carbon estimations determined by satellite imagery are significantly lower than drone estimations

Above ground biomass maps were produced for each drone DEM, and the mean AGB

value was taken from each grid sample to compare against SRTM samples. From all the drone

data, there was a mean of 73.52 ± 20.04 Mg/ha per sample. Conversely, 9.49 ± 10.68 Mg/ha was

calculated per sample from the SRTM data. The cumulative biomass estimated from drone and

SRTM was 12,249.45 and 1002.49 Mg respectively. Following the 0.451 conversion factor, there

was 5512.25 and 451.12 Mg of above ground carbon storage found for drones and SRTM. These

data are described in Table 2.1. Total biomass estimated by drone is over 12 orders of

magnitudes greater than SRTM estimated biomass. As a result, carbon storage is also underestimated by SRTM data by the same factor. The frequency distribution of the biomass samples (Figure 2.2a) shows SRTM data is clustered towards lower values and even appears to exponentially decrease past its mean value (9.49 Mg/ha). A Welch's t-test shows that the biomass by instrument have different means, and SRTM calculated AGB is significantly lower than drone AGB. As carbon is proportionally related to AGB, satellite estimated carbon also significantly lower by at least 1 order of magnitude. As described in the previous sections, estimated canopy height and mangrove extent were significantly different from each other by instrument each time. Figure 2.2b-c show an example biomass map from one of the most fragmented site in our study, visually representing how much lower SRTM estimated biomass is compared to the drone results.

Table 2.1: Summary of results

The main results for biomass comparisons by instrument.

	Drone	Satellite
# samples	3,047	1,232
Total Area (ha)	168.31	106.76
Mean AGB (Mg/ha)	73.52 ± 20.04	9.49 ± 10.68
Total Estimated AGB (Mg)	12,249.45	1002.49
Total Above Ground Carbon (Mg)	5512.25	451.12

Figure 2.2: Differences in estimated AGB by instrument

Comparison of biomass results from drone and SRTM data. (a) Frequency distribution of mean estimated AGB per grid for all samples. Green represents SRTM samples and yellow are drone sampels. The dashed lines represent the mean AGB across all samples, 73.52 ± 20.04 Mg/ha for drone and 9.49 ± 10.68. The mean AGB by instrument are significantly different from each other. (b) SRTM map of AGB from one site in La Paz 2018. The mean biomass per sample was 20.91 ± 10.33 Mg/ha. (c) Drone map of AGB from the corresponding site, and the mean biomass per sample was 5.45 ± 8.76 Mg/ha.
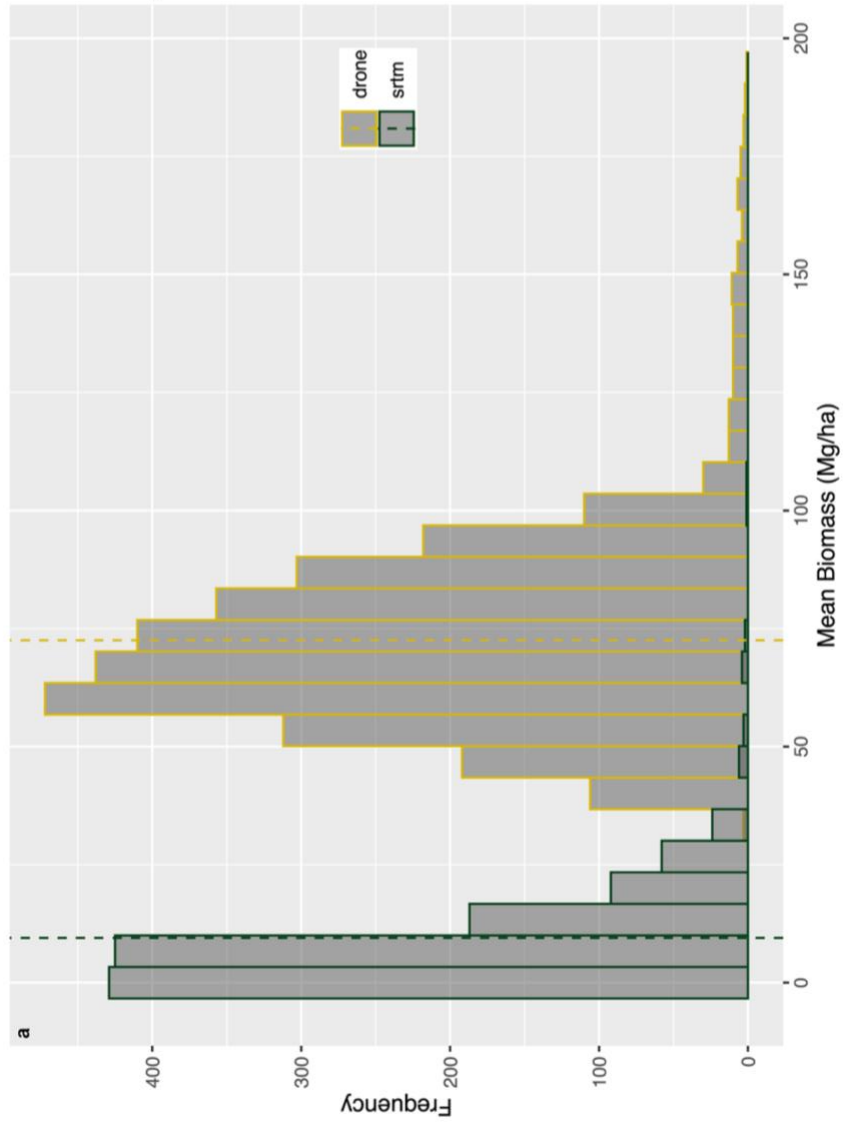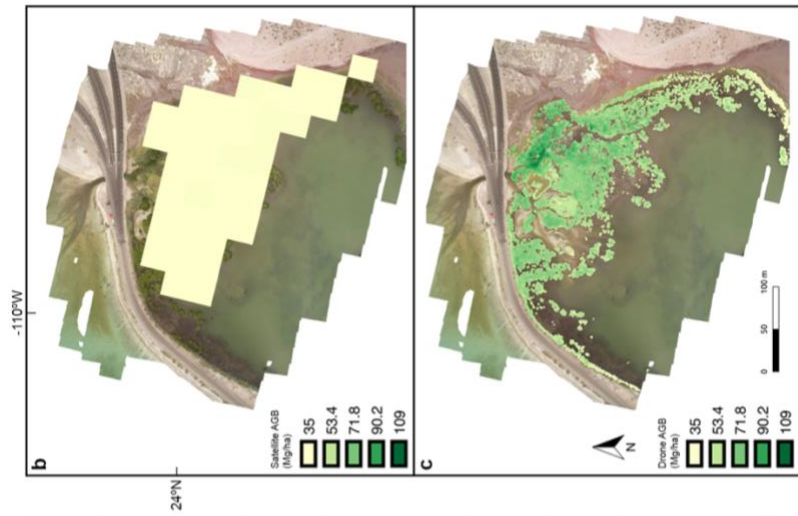
<u>Removing edge cases still shows a significant difference in biomass for type of instrument used</u>

The complete grids were also analyzed to verify the significant difference between biomass results by instrument. These samples were only taken when a 30x30m grid fully covered the corresponding section of the mangrove extent from the drone data. This was to ensure complete overlap with drone and SRTM biomass estimates, and there were only 150 samples that fulfilled this condition. The number of samples across site varied as highly fragmented sites would have many intersections from non-mangrove classes, which cause them to be excluded from the dataset. A histogram of the completely overlapping samples per instrument still showed the SRTM samples highly right skewed, with a mean of 10.76 ± 11.42 Mg/ha (Graph 2.5). Biomass from drone samples resulted in a mean of 80.70 ± 22.17 Mg/ha. There was a significant difference between the means of drone and SRTM calculated AGB (Welch's t-test; p-value $\ll$ 0.01). Removing edge cases with differences in labelled extent did not significantly change the results of biomass differences from drone and SRTM data.

Graph 2.5: Frequency distribution of completely overlapping samples by instrument

A histogram of mean AGB per sample grouped by instrument. The red represents drone data, and the blue is SRTM. The dashed lines represent the mean of each distribution: 10.76 ± 11.42 Mg/ha for SRTM and 80.70 ± 22.17 Mg/ha for drone.
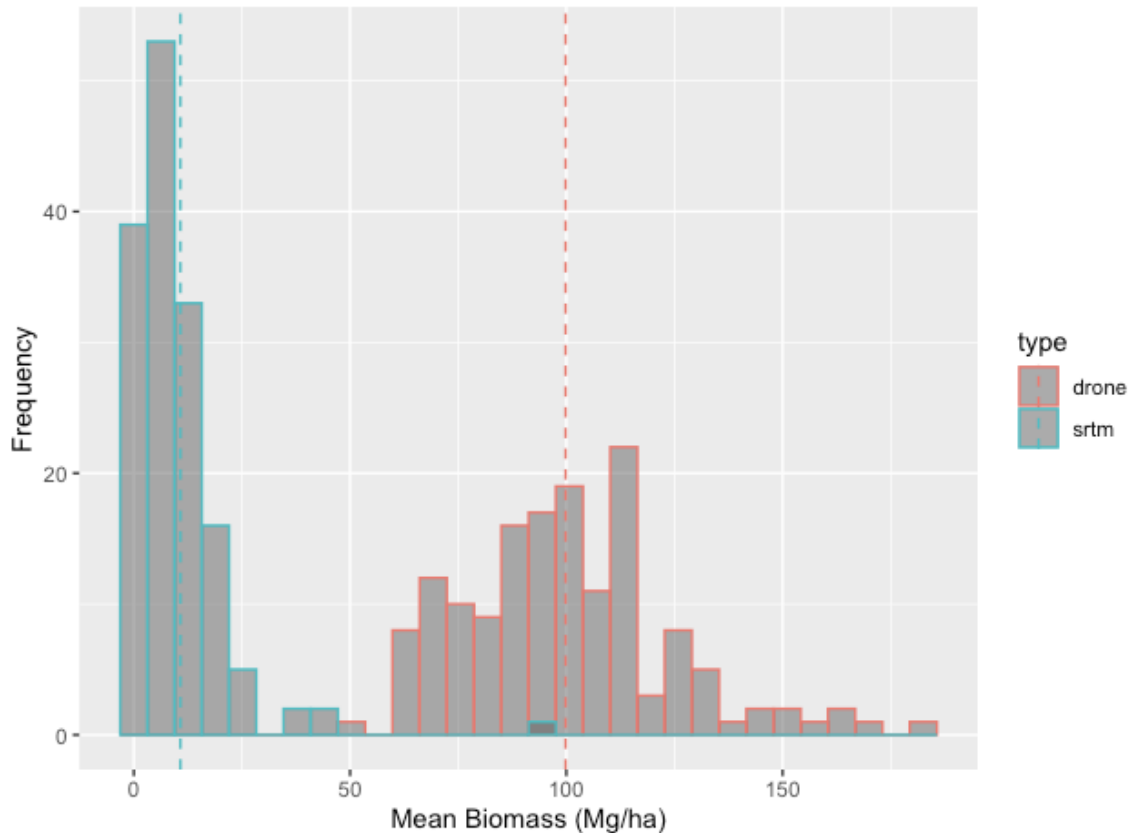
<u>Satellite and drone estimated biomass have different results between size classes</u>

AGB estimates are influenced by the amount of mangrove extent and estimated canopy height for our models. Because site size was a factor that significantly affected measured extent by instrument, it was also tested as a potential variable for affecting biomass. Total biomass was summed across all samples for each site and organized in increasing order (Graph 2.6a). Drone estimated AGB appeared to grow exponentially as area increased, while SRTM biomass did not appear to show any trends. After grouping sites into their assigned size classes, this relationship

50

became more distinct as drone estimated biomass were clearly increasing from one size to another (Graph 2.6b). The total biomass for SRTM data did not show the same pattern and remained consistently low across each size class.
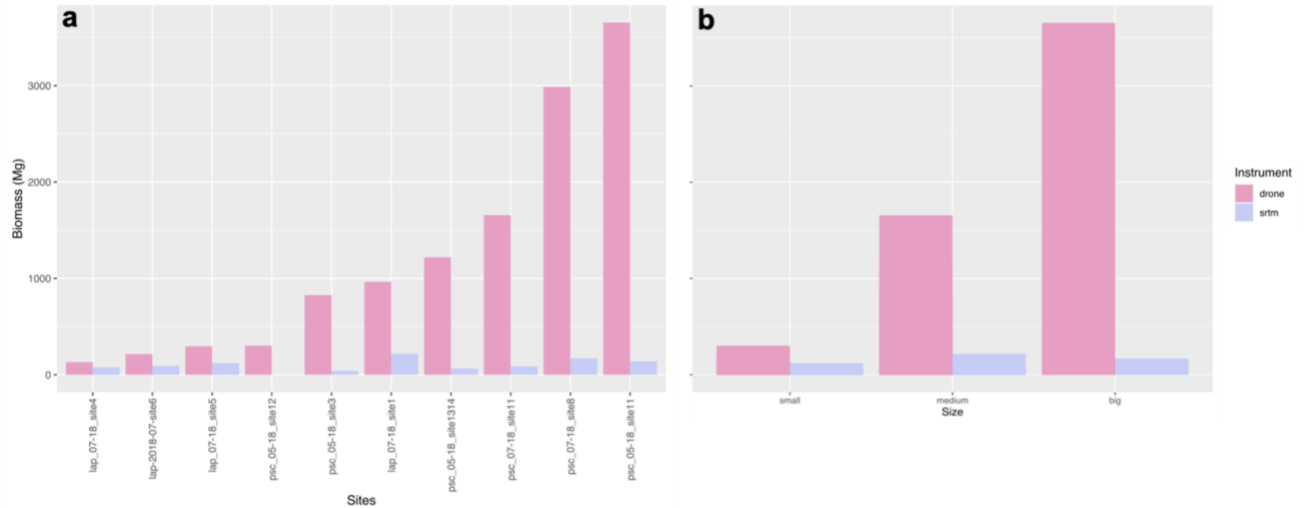
Graph 2.6: Total biomass by site and size class for drone and SRTM results

(a) Cumulative AGB (Mg) for each site in increasing order of drone area. Pink represents drone data and purple is SRTM. (b) Summed AGB (Mg) for each size class by instrument.

Square root transformations were applied on the mean biomass totals to maintian normality and equal varianc A two-way ANOVA was conducted using size class and type of instrument as factors. There was a significant interaction effect found (p-value $\ll 0.001$) for the two categories. A post-hoc Tukey test determined which groups were significantly different from each other, labelling them by letters to indicate similar and different groups (Graph 2.7). Small, medium, and big sites were all significantly different from each other for biomass estimated by drone. None of the SRTM biomass means per size class were significantly different from each other. For the small class, drone and SRTM biomass means were not significantly different.

51

Graph 2.7: Results of Tukey test for biomass estimates by size class and instrument

Drone and SRTM biomass means for small, medium, and big size sites. Different letters represent groups that are significantly different from each other. The post-hoc test grouped the following together: small SRTM, small drone, medium SRTM, big SRTM; medium drone; big drone.

Biomass Means by Site and Instrument
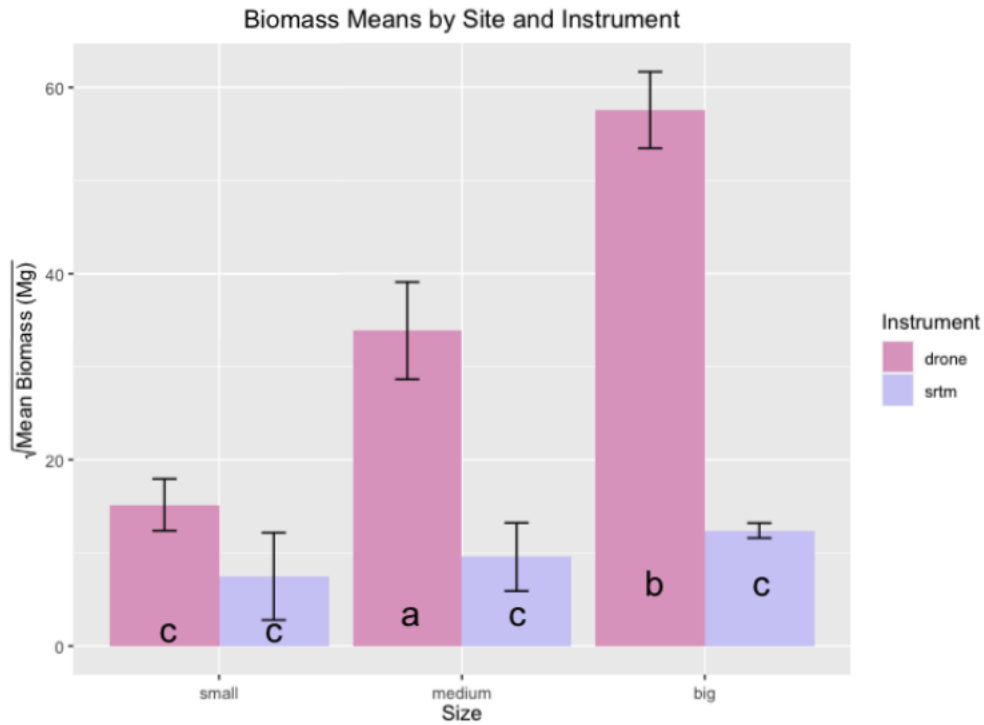
DISCUSSION

<u>Error from satellite area estimation increases as mangrove extent increases</u>

Measured mangrove extent is dependent on the labels generated for classifying mangrove from models, and the resolution of imagery used. For our drone models, annotators were trained for multiple sessions before labelling data for this study. Sections of orthomosaics were sometimes labelled several times to check for consistency and accuracy, and each site was reviewed by experts by referencing the higher resolution 10m imagery for quality assurance. Although manual labelling was rigorous and time consuming, it was critical for establishing an

accurate baseline for estimating biomass and analyzing satellite results. The study that produced the global mangrove study utilized labels generated from digital classifications by supervised and unsupervised learning. These were at a 30 m resolution scale and verified using high resolution satellite data from Google Earth (Giri et al. 2011). Due to the differences in labelling methods and pixel size for models, measured mangrove extent varied across these datasets.

Because the drone produced labels were meticulously cross-verified multiple times for correctness, they were determined to be representative of true mangrove extent for the surveyed sites and used to assess the accuracy of SRTM results. Surprisingly, there was no significant difference observed between the means of the all the combined sites for each instrument. This was likely due to the resolution of SRTM as the larger pixel sizes would often blur into non-mangrove classes. As a result, mangrove extent was sometimes under- or over-estimated by the satellite and relatively balanced out. Using the drone labelled extent as a baseline for establishing size classes, the discrepancies in measured extent was elucidated between drone and SRTM. The results indicated that area estimation by size class is dependent on the instrument used. SRTM data ranged from minorly underestimating or even overestimating area for small sites to significantly underestimating extent in big sites. SRTM extent seemed to do well in the small and medium sites, though the medium and small SRTM areas were not significantly different. For the big sites, which were greater than 20 ha, SRTM measured extent was significantly lower than the drone's. From our results, the amount of mangrove area mapped by SRTM is more accurate for smaller sized forests than larger ones. The big forests are underestimated by over 15 ha, which can potentially impact biomass results.

In this study, only the amount of coverage for mangrove area was analyzed in relation to biomass. SRTM models could detect similar amounts of area as the drone could for small to

medium forests, but the 30 m would often include non-mangrove areas (Figure 2.1c-d). The

addition of non-mangrove groups, such as other vegetation or abiotic sources, can reduce the

accuracy of biomass and carbon estimations. In the 2011 study that generated the global

mangrove extent map (Giri et al.), 'true mangrove' was defined as trees, shrubs, and palms

growing in tidal and intertidal zones. However, they were unable to statistically verify the

validity of the labels due to the lack of detailed global mangrove labels. We detected at least

17.68 ha, or 16.56%, of true non-mangrove extent that were classified as mangrove by SRTM

from all of our sites combined. Thus, satellite imagery correctly labelled mangrove extent for

only 83.44% of all our sites. However, SRTM mislabeled $25.48 \pm 18.83\%$ on average per site.

The potential implications of misclassifying mangroves could affect how canopy height is

estimated, which would directly affect biomass and carbon results. This study does not

statistically analyze the accuracy of SRTM results, but drone imagery can be used to validate

satellite data and even correct for its errors in classification to better monitor mangrove stocks in

future experiments. One study used drone measured mangrove extent to derive correction factors

for multiple datasets labelled from satellite imagery (Hsu et al. 2020). By pairing these

instruments, studying mangrove forests by remote sensing can be improved for local

management and conservation efforts.

<u>Canopy height estimations are controlled by spatial resolution</u>

Maximum drone values per 30m sample were compared against $SRTMH_{max}$ values, and

these values were reported to be significantly different. Similarly to mangrove extent, SRTM

canopy height values were also underestimated as the mean canopy height per sample was over

2x in magnitude less than the drone measurements for drone. This aligns with the reported error

for the global dataset we downloaded the SRTMH$_{max}$ maps from, which calculated an RMSE of

6.31 m for in situ measurements and 5.7 m for the regression with GLAS (Simard et al. 2019).

This is greater than the reported RMSE value of 0.54 m for the drone altimeter results with in

situ data. Furthermore, areas that were estimated to have an elevation of 0 m but classified as

mangrove were given a default value of 0.5 m. These factors contribute to the underestimations

by satellite imagery as well, which may be propagated by incorrect mangrove labels as discussed

previously. Nonetheless, these values are more accurate than previously established baselines of

global mangrove height (Rodriguez et al. 2006). However, the dwarf mangrove forests in BCS

are typically under 6m total, so the errors from the SRTMH$_{max}$ values would substantially impact

results from this region. Therefore, drones are advantageous for conducting surveys in these

forests or verifying satellite data.

Size class had no significant main or interaction effect on estimated height, and the

primary driver for height was the type of instrument used. This is expected as the area of a forest

was not a hydrological parameter that significantly affected canopy height distribution in Chapter

1. Thus, differences in canopy height were caused by differences between drone and SRTM data.

Because the spatial resolution of satellite imagery is almost 1000x worse, capturing topography

for shorter, fragmented forests is difficult as pixels can overlap into non-mangrove classes and

skew the results. As described in the previous section, SRTM pixels can be misclassified, and the

majority of a site can sometimes be represented by soil, water, or non-mangrove vegetation

instead of actual mangrove extent. Additionally, the distance from the satellite to tree tops is

much farther than drone drones (120 m), reflectance and atmospheric conditions can have a

larger effect on height estimations. Due to the caveats in satellite data, their corresponding

canopy height results have a higher error range and can potentially affect biomass and carbon calculations.

Biomass for dwarf mangroves is severely underestimated by satellite imagery

We found that satellite imagery underestimates AGB and consequently carbon by at least 1 order of magnitude. Total area of mangrove extent directly influences how much biomass is estimated since larger areas represent more mangrove coverage, which typically suggest more trees and above ground biomass. However, drone estimated biomass is linearly derived from canopy height, so lower detected values for height are translated into smaller amounts of AGB per pixel. Thus, sites with larger estimated forest coverage but shorter trees may have less biomass and carbon storage than smaller sites with tall trees. Our results suggest that area and instrument have a significant interaction effect on detected biomass, so the biomass estimations by size class are dependent on the type technology used. The post-hoc test reveals that small, medium, and big sites all have significantly different amounts of biomass calculated from the drone DEMs (Figure 2.10). Because more observed mangrove extent indicates larger forests, this result is expected as a larger quantity of trees can contribute to more biomass.

Biomass for SRTM results were generated from basal area weighted height maps, which is a linear transformation from the SRTM height. The allometric equation for biomass was generated from a non-linear regression across North, Central, and South America, and had an RMSE of 3.6 m. Interestingly, the SRTM models did not have significant differences between any of their size classes. In other words, biomass levels for this instrument remain constant even as the size forests increases. Though there was no significant effect on canopy height estimations with size class, there is a visible inverse relationship with mean canopy height and size class for

SRTM data (Graph 2.4b). The lower canopy height values likely contributed to the insignificant increases in SRTM biomass, resulting in similar means across the size classes. Comparing by instrument, drone and SRTM biomass were significantly different from each other at each size except for small, implying that SRTM estimates biomass more closely to the drone for sites under 5 ha in area. Though our study site was only focused in BCS, satellite imagery likely underestimates other dwarf mangrove areas which may significantly contribute to global stocks of biomass and carbon. This can have implications on local management for these smaller forests, as their ecosystem contributions are likely undervalued.

Given that the drone DEMs and labels are accurate and representative of true mangrove structure, their biomass results as baselines for establishing forest stocks. Using the IPCC recommended conversion factor, above ground carbon storage was calculated from AGB. Carbon estimates were also underestimated by over 12 orders of magnitude by SRTM data because carbon is a direct proportion of biomass. However, below ground biomass and carbon were not included as our field work did not conduct sampling for roots. Mangroves are known for their large stores of carbon underground, especially in scrub and arid forests (Virgulino-Júnior et al. 2020; Ezcurra et al. 2015). Below ground biomass can account for up to over half or more of total biomass and can be related to soil carbon stock (Saintilan 1997; Hiraishi et al. 2014; Virgulino-Júnior et al. 2020). In future work, below ground biomass and carbon allometric equations can be derived and added to above ground stocks for a more comprehensive understanding of total forest inventory. These data would inform researchers on how mangroves change over time and in response to stressors, providing insight on potential shifts in ecosystem structure and contribution.

Drones are better equipped to survey fragmented, shorter mangrove forests

Though drones significantly enhance the accuracy of determining mangrove coverage, they are not always feasible to use for certain experiments. Large scale studies that can span multiple countries rely on data that has high coverage and range. Collecting data via drone requires flying over whole forests to take imagery, and cross referencing with higher resolution imagery. From our field work, flights could sometimes take up to an hour and use up multiple batteries for bigger sites. However, they are a powerful tool that can be used to conduct regional scale experiments with a very fine level of detail. Subtle spatial variations and topographic features can be captured with drones, and measuring parameters like coastal fractality and distance to nearest water become possible at high resolution. The fragmentation of forests is typically eclipsed by satellite imagery, and water distance is dependent on pixel size. These variables have significant effects on canopy height distribution in the BCS sites, which is directly linked to biomass and carbon estimations. By interpreting how these factors have a role in mangrove ecosystems, dwarf forests in arid climates can be further understood for their ecological roles and functions. Furthermore, as more flights and data are collected, more sites can be included in this work and to further compare satellite and drone differences. Drones may offer more insight and potentially allow for correction factors in biomass, which would greatly expand the extent of available data. Inclusion of other sites and different forest types would allow for more understanding of how mangroves respond to climate change and tropicalization effects, giving scientist and policymakers information to anticipate shifts in wetlands structure. These tools are for not only suitable for monitoring current forest dynamics but also comprehending imminent consequences of anthropogenic induced climate change, deforestation, and detriment to biota health.

This study spanned several datasets and was collected through multiple trips over time, so it is expected that several sources of error were introduced into our results. Drone data was collected in May and June of 2018, while data from the global mangrove study spanned multiple years. The SRTM DEM used imagery from 2000; GLAS data used baseline measurements from 2003-2009; and field data was collected from 2004-2016. As a sizable amount of time had passed between measurements, there are likely changes from mangrove growth and deterioration from the years. However, a study had analyzed differences from SRTM, lidar, and field data to suggest that the SRTM height is tolerable to these changes and remains constant enough over time for canopy height measurements in settled mangroves (Lagomasino et al. 2016; Simard et al. 2019). In this case, the satellite resolution was advantageous in maintaining consistency over the years. Additionally, an analysis by Global Mangrove Watch estimated that mangrove extent in Mexico has decreased by 855.52 km^2 (85,552 ha) from 1996 to 2016 (Bunting et al. 2018). If this decrease was relatively consistent throughout the country, it is possible that the measured mangrove extent from 2000 is an overestimation or similar to the extent in 2018. Nonetheless, this is the most current global baseline of mangrove biomass distribution. As remote sensing techniques continue to advance and global maps are updated, comparisons against more recent data can be run to ensure better alignment.

Conclusions

This study completed a direct comparison of drone and SRTM data and revealed differences in contributors to above ground biomass estimates. With the high level of detail and multiple verifications for accuracy, drone mangrove extent was used as a baseline for analyzing SRTM results. Mangrove extent had significant differences by instrument and size,

demonstrating that error in satellite measured area increased as site size increased. This signified that SRTM data over- and under-estimated mangrove extent, as determined by the proportion of incorrectly labelled true non-mangrove area. Canopy height was also underestimated primarily due to the instrument type, and size did not have a significant effect on height estimations. 12,249.45 Mg of biomass and 5512.25 Mg of carbon were calculated with drone imagery from the 10 surveyed sites, while 1002.49 Mg of biomass and 451.12 Mg of carbon were detected from SRTM models. Biomass and carbon storage also depended on size of site and instrument used, as increasing size classes did not significantly distinguish mean SRTM biomass measurements from each other. Given the nature of fragmented, dwarf mangroves in desert habitats, drones serve as a more robust tool for monitoring regional changes. Paired together, drones and satellites can be used to expand datasets and verify each other in large scale studies.

Chapter 2, in part, is currently being prepared for submission for publication of the material. Qi, Katherine; Hsu, Astrid; Aburto, Octavio; Kastner, Ryan.

REFERENCES

Acosta-Velázquez, J.; Vázquez-Lule, A.D. Caracterización del sitio de manglar Bahía Magdalena, en Comisión Nacional para el Conocimiento y Uso de la Biodiversidad (CONABIO). 2009. Available online: http://www.conabio.gob.mx/conocimiento/manglares/doctos/caracterizacion/PN03_Bahia_Magdalena_caracterizacion.pdf (accessed on 11 July 2021).

Alongi, Daniel M. 2002. "Present State and Future of the World's Mangrove Forests." *Environmental Conservation* 29 (3): 331–49. https://doi.org/10.1017/S0376892902000231.

Bryan-Brown, Dale N., Rod M. Connolly, Daniel R. Richards, Fernanda Adame, Daniel A. Friess, and Christopher J. Brown. 2020. "Global Trends in Mangrove Forest Fragmentation." *Scientific Reports* 10 (1): 7117. https://doi.org/10.1038/s41598-020-63880-1

Bunting, Pete, Ake Rosenqvist, Richard Lucas, Lisa-Maria Rebelo, Lammert Hilarides, Nathan Thomas, Andy Hardy, Takuya Itoh, Masanobu Shimada, and C. Finlayson. 2018. "The Global Mangrove Watch—A New 2010 Global Baseline of Mangrove Extent." *Remote Sensing* 10 (10): 1669. https://doi.org/10.3390/rs10101669.

Carr, James R., and William B. Benzer. 1991. "On the Practice of Estimating Fractal Dimension." *Mathematical Geology* 23 (7): 945–58. https://doi.org/10.1007/BF02066734.

Cavanaugh, K. C., J. R. Kellner, A. J. Forde, D. S. Gruner, J. D. Parker, W. Rodriguez, and I. C. Feller. 2014. "Poleward Expansion of Mangroves Is a Threshold Response to Decreased Frequency of Extreme Cold Events." *Proceedings of the National Academy of Sciences* 111 (2): 723–27. https://doi.org/10.1073/pnas.1315800111.

Chmura, Gail L., Shimon C. Anisfeld, Donald R. Cahoon, and James C. Lynch. 2003. "Global Carbon Sequestration in Tidal, Saline Wetland Soils." *Global Biogeochemical Cycles* 17 (4): n/a-n/a. https://doi.org/10.1029/2002GB001917.

Cintron, Gilberto, Ariel E. Lugo, Douglas J. Pool, and Greg Morris. 1978. "Mangroves of Arid Environments in Puerto Rico and Adjacent Islands." *Biotropica* 10 (2): 110. https://doi.org/10.2307/2388013.

CONAGUA (2011) Estadísticas del agua en México. Ed. 2011. Comisión Nacional del Agua. Insurgentes Sur No. 2416, Col. Copilco el Bajo C.P. 04340, Coyoacán, México, D.F. Available at: http://www.conagua.gob.mx (accessed 20 October 2011).

Corte, Guilherme N., Helio H. Checon, Yasmina Shah Esmaeili, Jonathan S. Lefcheck, and A. Cecília Z. Amaral. 2021. "Mangrove Fragments as Key Coastal Reservoirs of Taxonomic and Functional Biodiversity." *Biodiversity and Conservation* 30 (5): 1573–93. https://doi.org/10.1007/s10531-021-02158-y.

Donato, Daniel C., J. Boone Kauffman, Daniel Murdiyarso, Sofyan Kurnianto, Melanie Stidham, and Markku Kanninen. 2011. "Mangroves among the Most Carbon-Rich Forests in the Tropics." *Nature Geoscience* 4 (5): 293–97. https://doi.org/10.1038/ngeo1123.

Ezcurra, Paula, Exequiel Ezcurra, Pedro P. Garcillán, Matthew T. Costa, and Octavio Aburto-Oropeza. 2016. "Coastal Landforms and Accumulation of Mangrove Peat Increase Carbon Sequestration and Storage." *Proceedings of the National Academy of Sciences* 113 (16): 4404–9. https://doi.org/10.1073/pnas.1519774113.

Fatoyinbo, Temilola E., and Marc Simard. 2013. "Height and Biomass of Mangroves in Africa from ICESat/GLAS and SRTM." *International Journal of Remote Sensing* 34 (2): 668–81. https://doi.org/10.1080/01431161.2012.712224.

Fazlioglu, Fatih, Justin S. H. Wan, and Luzhen Chen. 2020. "Latitudinal Shifts in Mangrove Species Worldwide: Evidence from Historical Occurrence Records." *Hydrobiologia* 847 (19): 4111–23. https://doi.org/10.1007/s10750-020-04403-x.

Funes-Rodríguez, R.; Gómez-Gutiérrez, J.; Palomares-García, R. *Estudios Ecológicos en Bahía Magdalena*; Centro Interdisciplinario de Ciencias Marinas, Instituto Politécnico Nacional: La Paz, Mexico, 2007.

Giri, C., E. Ochieng, L. L. Tieszen, Z. Zhu, A. Singh, T. Loveland, J. Masek, and N. Duke. 2011. "Status and Distribution of Mangrove Forests of the World Using Earth Observation Satellite Data: Status and Distributions of Global Mangroves." *Global Ecology and Biogeography* 20 (1): 154–59. https://doi.org/10.1111/j.1466-8238.2010.00584.x.

Hazra, Sugata, Anirban Mukhopadhyay, Abhra Chanda, Parimal Mondal, Tuhin Ghosh, Sandip Mukherjee, and Mashfiqus Salehin. 2016. "Characterizing the 2D Shape Complexity Dynamics of the Islands of Sundarbans, Bangladesh: A Fractal Dimension Approach." *Environmental Earth Sciences* 75 (20): 1367. https://doi.org/10.1007/s12665-016-6175-3.

Hiraishi, Takahiko, Thelma Krug, Kiyoto Tanabe, Nalin Srivastava, Baasansuren Jamsranjav, Maya Fukuda, and Tiffany Troxler. 2014. "2013 Supplement to the 2006 IPCC Guidelines for National Greenhouse Gas Inventories: Wetlands. Methodological Guidance on Lands with Wet and Drained Soils, and Constructed Wetlands for Wastewater Treatment." IPCC. https://www.ipcc.ch/site/assets/uploads/2018/03/Wetlands_Supplement_Entire_Report.pdf.

Howard, Jennifer, Ariana Sutton-Grier, Dorothée Herr, Joan Kleypas, Emily Landis, Elizabeth Mcleod, Emily Pidgeon, and Stefanie Simpson. 2017. "Clarifying the Role of Coastal and Marine Systems in Climate Mitigation." *Frontiers in Ecology and the Environment* 15 (1): 42–50. https://doi.org/10.1002/fee.1451.

Hsu, Astrid J., Lo, Eric K, Dorian, John B, Guerrero Martinez, B. Drone Flight Manual: UCSD Mangrove Imaging Procedure (Version 1.3). https://escholarship.org/uc/item/2zv0z6zm (accessed on 11 July 2021).

Hsu, A. J.; Dorian, J. B.; Qi, K.; Lo, E. K.; and Guerrero Martinez, B. 2019. Drone Image Manual: UCSD Mangrove Image Processing (Version 1.2). University of California, San Diego, Centro para la Biodiversidad Marina y Conservación, and the Gulf of California Marine Program. San Diego, California, USA. (accessed on 11 July 2021).

Hsu, Astrid J., Joy Kumagai, Fabio Favoretto, John Dorian, Benigno Guerrero Martinez, and Octavio Aburto-Oropeza. 2020. "Driven by Drones: Improving Mangrove Extent Maps Using High-Resolution Remote Sensing." *Remote Sensing* 12 (23): 3986. https://doi.org/10.3390/rs12233986.

Jolly, Ian D., Kerryn L. McEwan, and Kate L. Holland. 2008. "A Review of Groundwater-Surface Water Interactions in Arid/Semi-Arid Wetlands and the Consequences of Salinity for Wetland Ecology." *Ecohydrology* 1 (1): 43–58. https://doi.org/10.1002/eco.6.

Jones, Alice R., Ramesh Raja Segaran, Kenneth D. Clarke, Michelle Waycott, William S. H. Goh, and Bronwyn M. Gillanders. 2020. "Estimating Mangrove Tree Biomass and Carbon Content: A Comparison of Forest Inventory Techniques and Drone Imagery." *Frontiers in Marine Science* 6 (January): 784. https://doi.org/10.3389/fmars.2019.00784.

Kanniah, Kasturi Devi, Chuen Siang Kang, Sahadev Sharma, and A. Aldrie Amir. 2021. "Remote Sensing to Study Mangrove Fragmentation and Its Impacts on Leaf Area Index and Gross Primary Productivity in the South of Peninsular Malaysia." *Remote Sensing* 13 (8): 1427. https://doi.org/10.3390/rs13081427.

Kruczynski W.L. & Fletcher P.J. (2012) Tropical Connections: South Florida's Marine Environment. IAN Press, University of Maryland Center for Environmental Science, Cambridge, MD, USA

Lagomasino, David, Temilola Fatoyinbo, SeungKuk Lee, Emanuelle Feliciano, Carl Trettin, and Marc Simard. 2016. "A Comparison of Mangrove Canopy Height Using Multiple Independent Measurements from Land, Air, and Space." *Remote Sensing* 8 (4): 327. https://doi.org/10.3390/rs8040327.

Li, M.S., L.J. Mao, W.J. Shen, S.Q. Liu, and A.S. Wei. 2013. "Change and Fragmentation Trends of Zhanjiang Mangrove Forests in Southern China Using Multi-Temporal Landsat Imagery (1977–2010)." *Estuarine, Coastal and Shelf Science* 130 (September): 111–20. https://doi.org/10.1016/j.ecss.2013.03.023.

Lugo, A E, and S C Snedaker. 1974. "The Ecology of Mangroves." *Annual Review of Ecology and Systematics* 5 (1): 39–64. https://doi.org/10.1146/annurev.es.05.110174.000351.

Mandelbrot, Benoit B. 1975. "Stochastic Models for the Earth's Relief, the Shape and the Fractal Dimension of the Coastlines, and the Number-Area Rule for Islands." *Proceedings of the National Academy of Sciences* 72 (10): 3825–28. https://doi.org/10.1073/pnas.72.10.3825.

Mcleod, Elizabeth, Gail L Chmura, Steven Bouillon, Rodney Salm, Mats Björk, Carlos M Duarte, Catherine E Lovelock, William H Schlesinger, and Brian R Silliman. 2011. "A Blueprint for Blue Carbon: Toward an Improved Understanding of the Role of Vegetated Coastal Habitats in Sequestering CO $_2$." *Frontiers in Ecology and the Environment* 9 (10): 552–60. https://doi.org/10.1890/110004.

Moberg, Fredrik, and Patrik Rönnbäck. 2003. "Ecosystem Services of the Tropical Seascape: Interactions, Substitutions and Restoration." *Ocean & Coastal Management* 46 (1–2): 27–46. https://doi.org/10.1016/S0964-5691(02)00119-9.

Pulver, Terry R. (1976) *Transplant techniques for sapling mangrove trees, Rhizophora mangle, Laguncularia racemosa, Avicennia germinans, in Florida.* St. Petersburg, FL, Florida Department of Natural Resources, Marine Research Laboratory, (Florida Marine Research Publications, 22)

Polidoro, Beth A., Kent E. Carpenter, Lorna Collins, Norman C. Duke, Aaron M. Ellison, Joanna C. Ellison, Elizabeth J. Farnsworth, Edwino S. Fernando, Kandasamy Kathiresan, Nico E. Koedam, Suzanne R. Livingstone, Toyohiko Miyagi, Gregg E. Moore, Vien Ngoc Nam, Jin Eong Oong, Jurgene H. Primavera, Severino G. Salmo III, Jonnell C. Sanciangco, Sukristijono Sukardjo, Yamin Wong, and Jean Wan Hong Yong. 2010. "The Loss of Species: Mangrove Extinction Risk and Geographic Areas of Global Concern." Edited by Dennis Marinus Hansen. *PLoS ONE* 5 (4): e10095. https://doi.org/10.1371/journal.pone.0010095.

Qi, Katherine. n.d. *UCSD E4E Biomass Mangrove*. https://github.com/UCSD-E4E/biomass-mangrove.

Rodríguez-Zúñiga, M.T., Troche-Souza, C., Vázquez-Lule, A.D., Márquez-Mendoza, J.D., Vázquez-Balderas, B., Valderrama-Landeros, L., Velázquez-Salazar, S., Cruz-López, M.I., Ressl, R., Uribe-Martínez, A., Cerdeira-Estrada, S., Acosta-Velázquez J., Díaz-Gallegos, J. Jímenez-Rosenberg, R., Fueyo-Mac Donald, L., y Galindo-Leal C. *Manglares de México/Extensión, Distribución y Monitoreo*; Comisión Nacional para el Conocimiento y Uso de la Biodiversidad: México, Mexico, 2013

Ridd, P.V., and T. Stieglitz. 2002. "Dry Season Salinity Changes in Arid Estuaries Fringed by Mangroves and Saltflats." *Estuarine, Coastal and Shelf Science* 54 (6): 1039–49. https://doi.org/10.1006/ecss.2001.0876.

Ruwaimana, Monika, Behara Satyanarayana, Viviana Otero, Aidy M. Muslim, Muhammad Syafiq A., Sulong Ibrahim, Dries Raymaekers, Nico Koedam, and Farid Dahdouh-Guebas. 2018. "The Advantages of Using Drones over Space-Borne Imagery in the Mapping of Mangrove Forests." Edited by Shijo Joseph. *PLOS ONE* 13 (7): e0200288. https://doi.org/10.1371/journal.pone.0200288.

Saintilan, N. 1997. "Above- and below-Ground Biomass of Mangroves in a Sub-Tropical Estuary." *Marine and Freshwater Research* 48 (7): 601. https://doi.org/10.1071/MF97009.

Saintilan, N., K. Rogers, D. Mazumder, and C. Woodroffe. 2013. "Allochthonous and Autochthonous Contributions to Carbon Accumulation and Carbon Store in Southeastern Australian Coastal Wetlands." *Estuarine, Coastal and Shelf Science* 128 (August): 84–92. https://doi.org/10.1016/j.ecss.2013.05.010.

Schmitz, N., E. Robert, Hamisi Ali Kirauni, and Nico Koedam. "Salinity fluctuations in mangrove forest of Gazi bay, Kenya: lessons for future research." (2009).

Simard, Marc, Lola Fatoyinbo, Charlotte Smetanka, Victor H. Rivera-Monroy, Edward Castañeda-Moya, Nathan Thomas, and Tom Van der Stocken. 2019. "Mangrove Canopy Height Globally Related to Precipitation, Temperature and Cyclone Frequency." *Nature Geoscience* 12 (1): 40–45. https://doi.org/10.1038/s41561-018-0279-1.

Simard, Marc, Keqi Zhang, Victor H. Rivera-Monroy, Michael S. Ross, Pablo L. Ruiz, Edward Castañeda-Moya, Robert R. Twilley, and Ernesto Rodriguez. 2006. "Mapping Height and Biomass of Mangrove Forests in Everglades National Park with SRTM Elevation Data." *Photogrammetric Engineering & Remote Sensing* 72 (3): 299–311. https://doi.org/10.14358/PERS.72.3.299.

Tran, Loi X ., and Andrew Fischer. 2017. "Spatiotemporal Changes and Fragmentation of Mangroves and Its Effects on Fish Diversity in Ca Mau Province (Vietnam)." *Journal of Coastal Conservation* 21 (3): 355–68. https://doi.org/10.1007/s11852-017-0513-9.

Twilley, Robert R., Victor H. Rivera-Monroy, Ronghua Chen, and Leonor Botero. 1999. "Adapting an Ecological Mangrove Model to Simulate Trajectories in Restoration Ecology." *Marine Pollution Bulletin* 37 (8–12): 404–19. https://doi.org/10.1016/S0025-326X(99)00137-X.

Valiela, Ivan, Jennifer L. Bowen, and Joanna K. York. 2001. "Mangrove Forests: One of the World's Threatened Major Tropical Environments." *BioScience* 51 (10): 807. https://doi.org/10.1641/0006-3568(2001)051[0807:MFOOTW]2.0.CO;2.

Vergés, Adriana, Peter D. Steinberg, Mark E. Hay, Alistair G. B. Poore, Alexandra H. Campbell, Enric Ballesteros, Kenneth L. Heck, David J. Booth, Melinda A. Coleman, David A. Feary, Will Figueira, Tim Langlois, Ezequiel M. Marzinelli, Toni Mizerek, Peter J. Mumby, Yohei Nakamura, Moninya Roughan, Erik van Sebille, Alex Sen Gupta, Dan A. Smale, Fiona Tomas, Thomas Wernberg, and Shaun Wilson. 2014. "The Tropicalization of Temperate Marine Ecosystems: Climate-Mediated Changes in Herbivory and Community Phase Shifts." *Proceedings of the Royal Society B: Biological Sciences* 281 (1789): 20140846. https://doi.org/10.1098/rspb.2014.0846.

Virgulino-Júnior, Paulo César Costa, Diego Novaes Carneiro, Wilson Rocha Nascimento, Michele Ferreira Cougo, and Marcus Emanuel Barroncas Fernandes. 2020. "Biomass and Carbon Estimation for Scrub Mangrove Forests and Examination of Their Allometric Associated Uncertainties." Edited by Mai-He Li. *PLOS ONE* 15 (3): e0230008.

Walters, Bradley B., Patrik Rönnbäck, John M. Kovacs, Beatrice Crona, Syed Ainul Hussain, Ruchi Badola, Jurgenne H. Primavera, Edward Barbier, and Farid Dahdouh-Guebas. 2008. "Ethnobiology, Socio-Economics and Management of Mangrove Forests: A Review." *Aquatic Botany* 89 (2): 220–36. https://doi.org/10.1016/j.aquabot.2008.02.009.

Westoby, M.J., J. Brasington, N.F. Glasser, M.J. Hambrey, and J.M. Reynolds. 2012. "'Structure-from-Motion' Photogrammetry: A Low-Cost, Effective Tool for Geoscience Applications." *Geomorphology* 179 (December): 300–314. https://doi.org/10.1016/j.geomorph.2012.08.021